

**Practical Experiments to Determine Performance Characteristics
of Shape Memory Alloys**

by

John Andrew Zulick, B.S.M.E.

Report

Presented to the Faculty of the Graduate School of

The University of Texas at Austin

in Partial Fulfillment

of the Requirements

for the Degree of

Master of Science in Engineering

The University of Texas at Austin

May 2000

DISTRIBUTION STATEMENT A
Approved for Public Release
Distribution Unlimited

200000710 058

DTIC QUALITY INSPECTED 4

Copyright
by
John Andrew Zulick
2000

DISTRIBUTION STATEMENT A
Approved for Public Release
Distribution Unlimited

**Approved by
Supervising Committee:**

J. B. Miller

AD NUMBER		DATE 15 JUNE 2000	DTIC ACCESSION NOTICE
1. REPORT IDENTIFYING INFORMATION			REQUESTER 1. Put your mailing on reverse of form 2. Complete items 3. Attach form to report mailed to DTIC 4. Use unclassified information on 5. Do not order documents for 6 to 8 weeks
A. ORIGINATING AGENCY Naval Postgraduate School, Monterey, CA 93943			
B. REPORT TITLE AND/OR NUMBER Practical Experiments To Determine Performance Characteristics Of Shape Memory Alloys			
C. MONITOR REPORT NUMBER By: John A. Zulick, Thesis, U of Texas, Austin, May 2000			
D. PREPARED UNDER CONTRACT NUMBER N62271-97-G-0073			DTIC: 1. Assign AD Number 2. Return to requester
2. DISTRIBUTION STATEMENT APPROVED FOR PUBLIC RELEASE; DISTRIBUTION UNLIMITED			

20000710 058

DTIC Form 50
JUL 96

PREVIOUS EDITIONS ARE OBSOLETE

Dedication

To my wife Barbara.

Acknowledgements

I am greatly indebted to the Andersen Consulting Professor of Manufacturing Systems Engineering for guidance and support received during my short stay at the University of Texas. I would especially like to thank Mr. Carey King, whose leadership and focus made this report possible.

May 2000

Abstract

Practical Experiments to Determine Performance Characteristics of Shape Memory Alloys

John Andrew Zulick, MSME

The University of Texas at Austin, 2000

Supervisor: Joseph J. Beaman

This report presents the design and operation of an experimental assembly to test and record properties of Shape Memory Alloy wire actuators. While the capabilities and varying properties of Shape Memory Alloys are many, this work focuses on transition temperatures and length changes in response to temperature and loading inputs. A brief background section on Shape Memory Alloys is presented, along with details of testing apparatus construction, experimental design, actual progress of experiments, and their summarized results.

Table of Contents

List of Tables.....	ix
List of Figures	xi
Chapter 1 Background.....	1
Shape Memory Alloy Characteristics	1
Commercial Applications.....	5
Alloy Shortcomings.....	6
Purpose for Experimentation.....	8
Assets and Constraints	9
Chapter 2 Testing Apparatus.....	10
Overall Requirements.....	10
Sample Assembly.....	11
Shape Memory Alloy Wires.....	11
Attachments and Fittings.....	12
Weight Application Lever and Fulcrum.....	13
Tensioning Crossbar.....	15
Temperature and Environmental Control.....	16
General Requirements	16
Environmental Chamber	17
Bottom Plate and Bottom Wire Attachment Point	17
Top Plate	19
Plastic Cylinder	19
Hot Plate.....	20
Heat Gun	21
Thermometer	22
Displacement Measurement	22
Optron.....	22

Oscilloscope	24
Displacement Transducer	24
Displacement Transducer Power Source.....	25
Testing Configurations	25
Chapter 3 Experimental Design	27
Statement of the Problem	27
Specific Variables to be Measured.....	28
Selection of Factors to be Varied	29
Choice of Factor Levels	30
Definition of Inference Space for the Problem	31
Number of Samples to be Taken	32
Number of Observations to be Taken	32
Order of Experimentation.....	33
Hypotheses to be Tested.....	34
Chapter 4 Experiments	35
Procedures and Sequence of Operations	35
General Observations	37
Difficulties Encountered and Their Resolution.....	38
Operations Conducted in Individual Experiments	42
Experiment #1	42
Experiment #2	43
Experiment #3	44
Chapter 5 Analysis	47
Introduction	47
Data Collection and Processing.....	47
Interpretation of Results	48
Hysteresis Curve	48
Elastic Behavior	51

Recovery of Strain With Heating	54
Loading Beyond Manufacturer Recommendations.....	54
Conclusions and Recommendations.....	55
Appendix A Manufacturer Data	57
Appendix B Calibration of Instruments	63
Appendix C Experimental Results	70
Bibliography	81
Vita	84

List of Tables

Table 1:	Young's Modulus Results Table.....	53
----------	------------------------------------	----

List of Figures

Figure 1:	Transition Pathways From Austenite to Martensite	2
Figure 2:	Hysteresis Curve	4
Figure 3:	Shape Memory Alloy Wire Sample Assembly	12
Figure 4:	Weight Application Lever and Fulcrum.....	14
Figure 5:	Tensioning Crossbar.....	15
Figure 6:	Bottom Plate and Bottom Wire Attachment Point	18
Figure 7:	Top Plate With Attachments	20
Figure 8:	Environmental Chamber Exploded View	21
Figure 9:	Wiring Configuration for Measurements With Optron.....	26
Figure 10:	Wiring Configuration for Measurements With Displacement Transducer	26
Figure 11:	Concept of the Failed Cooling Pan Idea.....	39
Figure 12:	Transition Temperatures for LT Series SMA Wires	48
Figure 13:	Transition Temperatures for HT Series SMA Wires	49

Chapter 1: Background: *Shape Memory Alloy*

Characteristics

Shape Memory Alloys (SMAs) are a special class of metals that can convert thermal energy directly into mechanical work due to a material transformation that occurs within the alloy. Called the Shape Memory Effect (SME), this diffusionless, solid-to-solid transformation occurs over a limited temperature range and changes the crystalline structure between two phases, a high temperature austenitic phase and a low temperature martensitic phase. (1) This report focuses on behavior of a particular class of Shape Memory Alloys, the nickel-titanium blend commonly referred to as "Ni-Ti."

Martensite inherits the composition and atomic order of the parent austenitic phase without changing the chemical nature of the matrix and also without the classic nucleation and growth seen in most other alloys. Microscopically, the metal's lattice structure stores and releases energy by allowing atoms to displace a small distance in relation to their neighbors in a cooperative rearrangement process during phase changes. These collective small displacements can add up to become large displacements and are indicated by changes in the metal's dimensions or shape at the macroscopic level. (2)

Cooling a Shape Memory Alloy will induce a forward transformation from austenite to martensite, and this transformation can also occur by loading. Metals undergoing a martensitic transformation do not require quenching to obtain

martensite, and if attempted, even the highest quench rates will not suppress formation of the martensitic low temperature phase. (2)(3) The reverse transformation changes martensite to austenite by heating, and if a recoverable amount of deformation has taken place while in a martensitic state, this transformation produces sought-after mechanical work in response to a temperature change. Figure 1 shows the relationship of these potential phase change paths in response to temperature or loading.

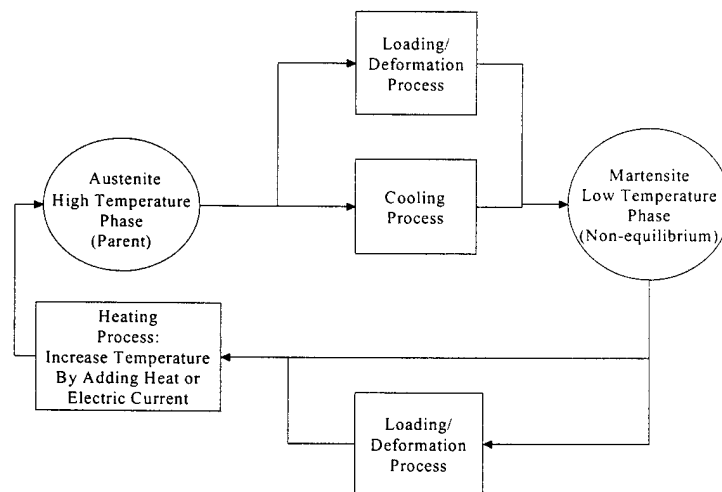


Figure 1: Transition pathways from austenite to martensite in a Shape Memory Alloy.

The ability of SMAs to respond quickly to temperature stimulus offers a possible avenue for solutions to engineering problems that involve an input of changing temperature and require an output of physical movement in response to that temperature change. Typically, metals will expand when exposed to an increase in temperature, but SMAs operate instead in contraction, a capability that

has intrigued engineers but which has proven difficult apply in practice. Over a range of 0°C - 100°C , common materials like copper, steel and aluminum display fairly linear and predictable expansion rates of 0.12% - 0.26% of total length that can be modeled by simple equations. (4) A Shape Memory Alloy, however, can change shape up to a maximum of 8.0% of total length for a similar change in temperature, but this change is nonlinear and difficult to model. Reduction to a 1.0% - 2.0% length change will permit cyclic action that can exceed 10^6 repetitions before the part loses the ability to regain its shape. Exceeding 8.0% strain will cause permanent plastic deformation that the Shape Memory Alloy cannot recover. (5)

During manufacture of Shape Memory Alloys, initial forming of the alloy's shape occurs at high temperatures where the parent austenitic phase dominates, and this initial shape is the 'remembered state.' As the alloy cools, the low temperature martensite phase appears. If the material is deformed in that low temperature martensitic state, the deformation will remain until sufficient heat is applied to transition the alloy through its hysteresis curve back to parent austenite. During this heating process, the alloy's shape returns to the 'remembered' austenitic state.(6) As shown in Figure 2, the greatest changes in shape and physical properties occur in the area of the alloy's hysteresis curve, with the metallurgical state of the alloy dependent on whether the alloy undergoes a heating process or a cooling process.

In addition to characteristically large recoverable strains that make SMAs attractive in mechanical actuator applications, SMAs have other advantages.

Shape Memory Alloy components will reset themselves after actuation to start a new cycle, can be miniaturized, operate independent of direction, are corrosion resistant, and are not affected by changing environmental conditions with the exception of temperature changes. There is no friction to account for in the alloy actuator itself as there would be in a linkage or bearing. The power density, or ratio of actuator output to actuator volume, is higher for SMAs than even hydraulic actuation. By using pulsed direct current inputs coupled with an appropriate cooling method and detailed knowledge of a specific alloy's response to inputs, control of Shape Memory actuator dimensions with tolerances of microns is possible. (8)

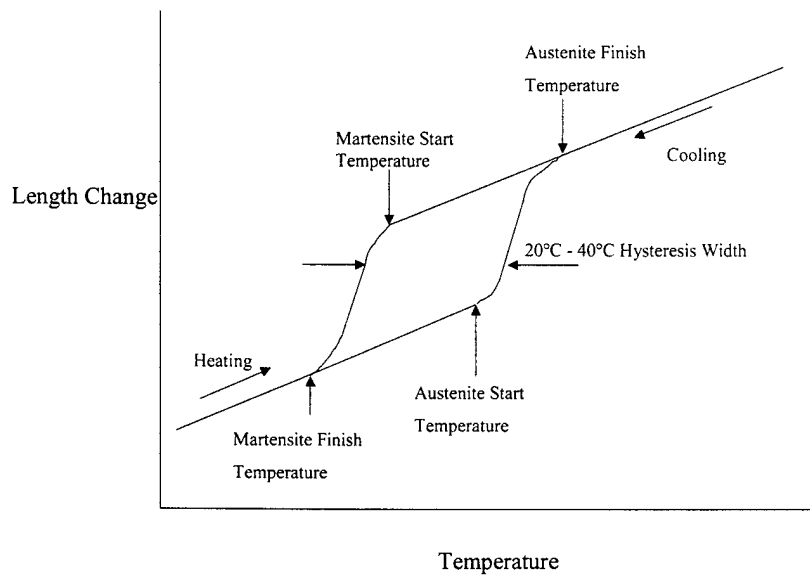


Figure 2: The hysteresis curve describes changes in physical properties as a function of temperature. (1-7)

COMMERCIAL APPLICATIONS

Commercial applications begin to show the versatility of Shape Memory Alloy components. Use of pipe couplings manufactured from SMAs in high pressure hydraulic systems greatly reduces installation time and costs because the SMA couplings can easily fit into confined areas, require no special tools to install, and their shrink fit bonds piping ends so tightly that welding and weld test equipment are not required. The SMA coupling is manufactured to dimensions slightly smaller than the pipe ends to be joined, cooled, and then mechanically expanded to a size that will easily slip over the pipe ends to be joined. The coupling is kept in a chilled state until ready for installation. After slipping the SMA coupling over the butted piping ends to be joined, the coupling is slowly heated and, as it transitions through the heating portion of the hysteresis curve, the coupling contracts to its original, smaller dimensions and creates a high strength shrink fit. (9)

Two applications in an expansion mode have the potential to replace conventional explosives. A Shape Memory Alloy is manufactured in a cylindrical shape and is then compressed to a smaller size, where it awaits actuation. The cylinder is inserted into a hole bored in concrete, where it undergoes heating and expands to its original, larger shape. The alloy's expansion imparts tons of stress in a confined area, exceeding the tensile strength of the surrounding concrete and causing fractures through a local area of the concrete volume. To reuse the SMA cylinder, it is removed from the bore hole and compressed in a specialized machine, after which it is ready to undergo another cycle. (10) In a related

application in the aerospace industry, a replacement is desired for explosive bolts which fire on command to separate two components joined tightly together. The explosive bolt is replaced by a conventional bolt, and washers made of SMAs are placed in the bolted connections. The washers expand on receiving input of a temperature change and the force generated by their expansion exceeds the rated tensile strength of the standard bolts, separating components without the disadvantages inherent in explosive components. (11)

In variable control applications, shape Memory Alloy wires with advanced sensors will alter airfoil configurations on leading and trailing edges of F-18 aircraft wings to reduce drag and match actual flight conditions. (12) Research is underway for SMA actuator use in helicopter blades to improve rotor aerodynamics and reduce vibration and noise by changing the shape of the rotor blade in response to flight control and environmental inputs. (13)

ALLOY SHORTCOMINGS

Despite the representative advances described above, integrating SMA capabilities into functional mechanisms proves difficult for a number of reasons. Although SMAs are finding wider applications, the majority are two position products where the SMA element starts in a temporary martensitic shape or position and deforms to its original austenitic shape upon heating. (14) These one-way applications are simple, allow increased dimensioning tolerances of SMA shapes, and do not require tight tolerances for heat input.

However, Shape Memory Alloys cannot tolerate short, high intensity bursts of energy and their use in control applications is hindered by the nonlinear

hysteresis behavior that permits high recoverable strains. Properties of the austenitic and martensitic phases differ greatly, with temperature and applied forces also affecting these properties. In Ni-Ti Shape Memory Alloys, the Nickel-Titanium ratio ranges from 49.0% - 50.7% Titanium, and the percentage of these alloying elements significantly affects SMA component properties. (15)

While undergoing transition, the alloys respond nonlinearly to temperature, and these responses change depending on whether the alloy is undergoing a heating or cooling processes. (16) Precise knowledge of the alloy state on the hysteresis curve is essential for developing accurate control schemes that intend to reverse the alloy's transition part way through a complete cycle. If reversal to a heating cycle is desired during a partially completed cooling cycle, heat must first be applied to transition completely across the 20°C - 40°C wide hysteresis gap to reach the heating portion of the curve shown in Figure 2 before any linear displacement can take place. Further heat addition will then move the alloy's state along the heating curve. This unusual delay in action may not be desirable in certain applications.

Tabular performance data for SMAs are not available as for common materials like steel or aluminum, and often only vendor information and testing in a particular application will define important SMA characteristics such as strain recoverability, electrical resistivity, and heat capacity as functions of input heat or electric current. (17)(18) Depending on the particular alloy, SMAs cost between \$1,000 and \$2,000 per kilogram. (19)

Before Shape Memory Alloys find widespread application, engineering solutions to the drawbacks described above will have to be found. If methods are developed to quickly cool SMAs and make them less costly to manufacture, their use in cyclic applications will become more attractive to commercial industry. (20) Advanced methods to sense the alloy's temperature during cycling would permit more accurate control, increase response speeds, and minimize electric current applied to the SMA part. Accurate control would in turn decrease energy consumption and limit alloy temperature to avoid overheating.(21) In the meantime, for those willing to expend the effort necessary to develop reliable designs with SMA components, the advantages of Shape Memory Alloys can provide great benefit.

PURPOSE FOR EXPERIMENTATION

An underwater mechanism with an onboard propulsion system was contemplated as part of another project. The small size, high power density, and ability of Shape Memory Alloys to function in an underwater environment indicated to the designer of this underwater system that Shape Memory Alloys had the potential to serve in the underwater device. Before committing to their use, however, questions remained on how much linear contraction could be extracted from a length of SMA wire, how much force the wire could exert, and what quantity of electric power would these actuators consume while providing motive force. Concurrent decisions regarding power sources, materials, geometry, and heat flow for the underwater device were dependent on reliable data obtained from available SMA actuators. To verify data obtained from

manufacturers and discover how the actuators performed in loaded conditions with varying temperatures, the decision was made to construct a device to conduct tests on alloy wires. The tests would also help verify a mathematical model for SMA behavior through its hysteresis. The mathematical model is beyond the scope of this report.

ASSETS AND CONSTRAINTS

Since this project was not funded by any outside source or within the local University Department, purchase of complete test equipment was not an available option and cost minimization was a paramount consideration. Existing test devices, measuring equipment and their accessories assigned to the University's Mechanical Engineering Department were employed wherever possible. Any additional parts required to complete the test assembly were machined from scrap using equipment in a Student Machine Shop. Specialized fittings and connectors were obtained from local supply sources.

Chapter 2: Testing Apparatus: *Overall Requirements*

To determine whether Shape Memory Alloys would serve as suitable mechanical actuators, the project's mission was to determine how much displacement could be obtained from Shape Memory Alloy wire actuators, at what temperatures, and under what loading conditions. The budget for the project was limited, so existing experimental and measuring devices were adapted to meet the project's needs, supplemented by commercially purchased fittings and custom machined components.

Primary considerations for developing a design for the apparatus were that the apparatus should be able to:

- Hold the wire steady with minimal displacement of the containing and measuring apparatus.
- Establish an enclosed environment surrounding the wire to control the temperature of air or water surrounding the wire.
- Add and remove heat in a controlled manner.
- Apply varying tensioning loads on the wire.
- Measure small displacements of the sample wire without interfering with the wire's expansion and contraction process.
- Permit easy insertion and removal of a wire sample.
- Measure the temperature of the wire or its environment.
- Allow clear visibility of the wire itself.

- Perform static testing with slow varying of temperature or applied mass, with the ability to use the experimental assembly in the future for dynamic testing, where the SMA wire receives an impulse of DC electric current and quickly changes shape in response to that impulse.

An existing pressure test vessel was pressed into service as an environmental control chamber for the wire samples as described below. Individual components were designed, machined, and assembled to meet test needs. The reader will note that, wherever possible, aluminum was used as construction material for the apparatus to maintain consistency of thermal expansion over temperatures planned to cycle from room temperature of 23°C to maximum test temperatures of 105°C. Screws and specialized fittings were manufactured primarily of steel. Specifications and operating ranges for equipment and fittings are listed in Appendix A.

SAMPLE ASSEMBLY: Shape Memory Alloy Wires

High temperature and low temperature Shape Memory Alloy wires were purchased from the Mondo-tronics Company of Encinas, California. The set of wires included 'Flexinol Muscle Wires' of two different Ni-Ti alloys, a Low Temperature grade and a High Temperature grade. The package included 200mm long wires of each grade in five different diameters: 37μm, 50μm, 100μm, 150μm, and 250μm. The manufacturer also supplied information on physical, electrical, force, speed, thermal, and material properties for the wires. (22)

Attachments and Fittings

Metal parts provided attachments for coupling the SMA wire to the experimental apparatus as shown in Figure 3. SMA wires were cut to lengths of approximately 90mm and then attached to 0.609mm diameter steel wires at both ends with metal connecting sleeves by mechanical crimping. The steel wires led to 34.4mm long swivel hooks of 1.27mm diameter steel wire which provided the ability to couple and uncouple the wire assembly to the experimental apparatus. After creating this SMA wire assembly, the effective length of the wire that would be free to move was measured before experiments and recorded. The overall length of this assembly was calculated so that, when attached to the lever arm, the wire assembly would be taut with the lever arm level.

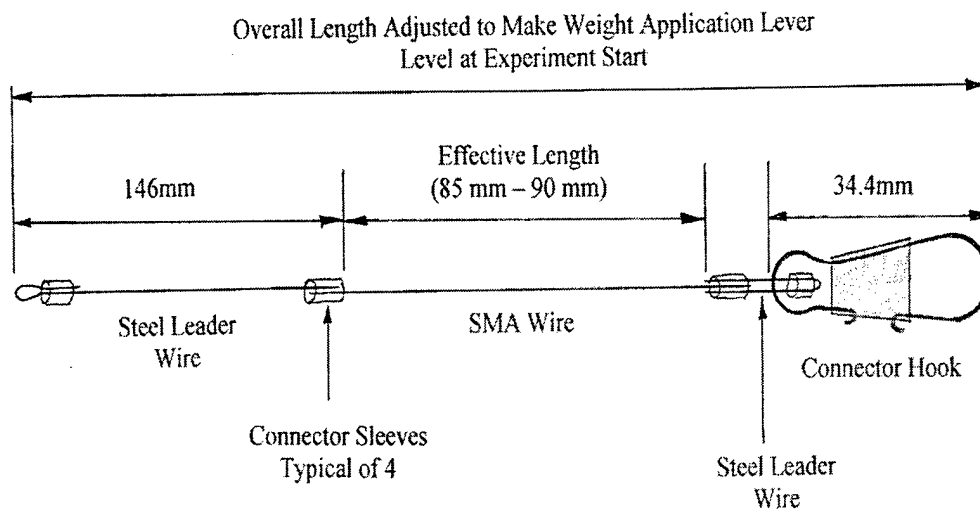


Figure 3: Shape Memory Alloy wire sample assembly as used in experiments.

WEIGHT APPLICATION LEVER AND FULCRUM

For each size of wires used in experiments, recovery forces varied from 20g to 2,000g, and a way needed to be found to apply forces of this range to a vertically oriented wire with minimal deformation of the surrounding apparatus. Because friction forces would be difficult to measure and control for such low levels of applied force, the design intended to minimize friction in a pivoting connection that transferred force from the input location at the weight stack to the wire location. High stiffness and low inertia for the lever were also desired to minimize measurement noise. To apply force to the SMA wire to tension it to full length during experiments and provide a way to measure its displacement accurately, a weight application lever and fulcrum were machined from aluminum scrap. The fulcrum was then attached to the top plate of the environmental container as shown in Figures 4 and 7.

The lever rests on the 90° machined angle at the apex of the fulcrum and supports connections for the SMA wire on one side and the weight application stack on the other. The lever itself balances evenly on the fulcrum when not loaded and can move in response to slight air current. The five holes on each side of the lever allow minor adjustments while aligning of the SMA wire assembly in the center of a hole in the top plate. Then, to maintain proper counter-balance, the attachment point of the weight stack can be positioned an identical distance from the fulcrum as the SMA wire's attachment point. This counter-balancing minimizes correctional calculations for how much force is actually applied to the

wire by the weight stack. The pivot point angle on the fulcrum where the lever rests is 90° , while the angle machined into the bottom of the lever measures 120° , allowing a gap of 15° on either side of the fulcrum for lever bar rotation. This gap will allow maximum displacement of 34mm at the lever's end. However, since the SMA wire will displace less than 10% of its effective length of 90mm during the course of experiments, the expected displacement seen by the lever at the point of attachment will be approximately 9mm, well within the lever's displacement capability.

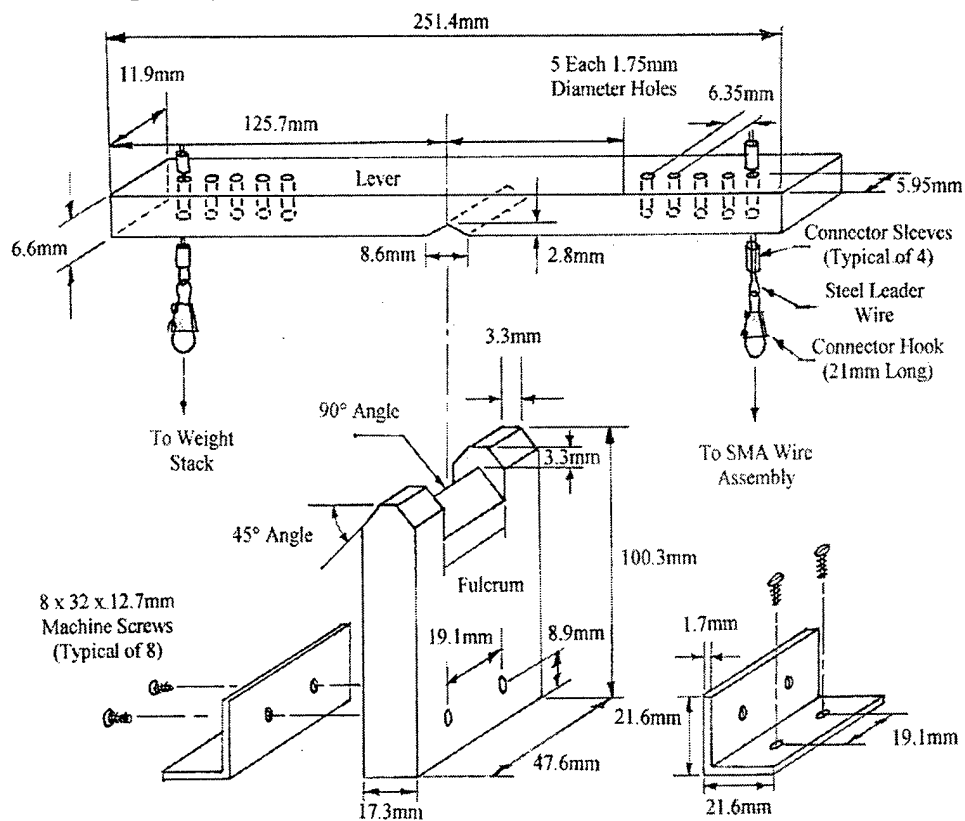


Figure 4: Weight application lever and fulcrum used to apply force to SMA wire.

TENSIONING CROSSBAR

The lever allows application of chosen masses to the SMA wire and works well for experiments where temperature or loads are varied slowly. Temperature changes of 1°C - 3°C per minute and application of a varying mass every 30 seconds allow the SMA wire to stabilize length without significant concern over dynamic friction present in the weight application assembly.

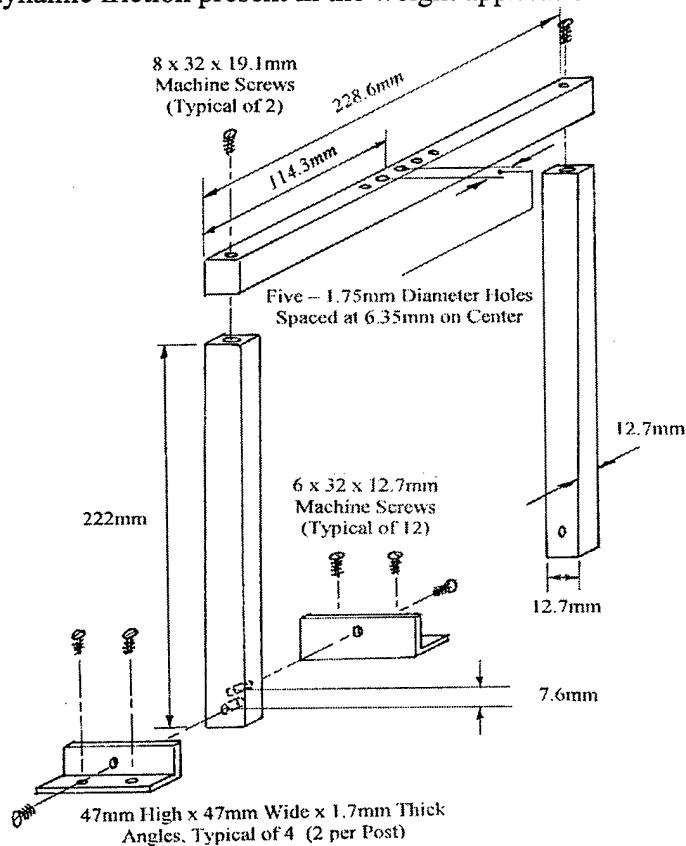


Figure 5: Tensioning crossbar and intended use for future dynamic testing.

To provide an opportunity for tensioning SMA wires during dynamic testing and eliminate the majority of concern over errors or experimental noise induced by friction or inertia, a tensioning crossbar was machined of zinc bar stock to provide a solid connection point for a metal spring that would in turn attach directly to the SMA wire sample assembly as shown in Figures 5 and 7. The tensioning crossbar assembly was not used during the course of experiments analyzed in this report.

TEMPERATURE AND ENVIRONMENTAL CONTROL:

General Requirements

To increase the accuracy of results, methods were required to input heat at the top and bottom plates to provide even temperature distribution inside the environmental chamber. SMA wire diameters of under 0.5mm made it impractical to attempt direct temperature measurement by attachment of a thermocouple or other sensor directly to the small wire. Issues of selection of bonding methods, impact of relatively inflexible bonding on a wire expected to undergo significant expansion and contraction, and measurement of temperature of a small volume wire complicated this problem. Scanning thermometers would have a very small target behind the 14mm thick plastic walls of the environmental chamber. As a solution to temperature measurement, two thermometers measured temperature at the middle and bottom regions of the environmental chamber, and their averages served as data points for experiments. Mixing of the air inside the chamber was aided by a rotating, plastic coated stirring rod under magnetic control of a hot plate.

Environmental Chamber

A device previously used for air pressure experiments was adapted for use as the SMA wire testing apparatus. The device consisted of a clear plastic cylinder with aluminum top and bottom plates secured by four steel threaded fasteners at the corners of the plates on the exterior of the cylinder. Rubber gaskets in grooved channels provided tight seals between the mating surfaces of the plastic cylinder and aluminum plates.

Bottom Plate and Bottom Wire Attachment Point

The bottom plate served as a heat conduction surface, a cooling surface, and a mounting surface for the SMA wire's bottom attachment point. To permit both rapid heating and cooling of the bottom plate, eight each 6.10mm wide grooves 7.60mm deep were machined across the length of the bottom surface to integrate a cooling coil with water as the thermal sink. A layer of thermal grease lined these gaps to increase heat transmission from the bottom plate to the embedded copper coils. The machined groove was deliberately cut 0.25mm thinner than the 6.35mm outer diameter of the thin wall copper tubing to force a slight press fit of the copper tubing, provide a tight seal for the grease, and slightly deform the tubing to increase the direct contact surface area between the tubing and the bottom plate. A 3.66m length of copper tubing was pre-bent using a standard tubing bender to form an 8-pass heat exchanger, and then tapped into place in the grooves with a rubber mallet. End fittings were standard gas system fittings.

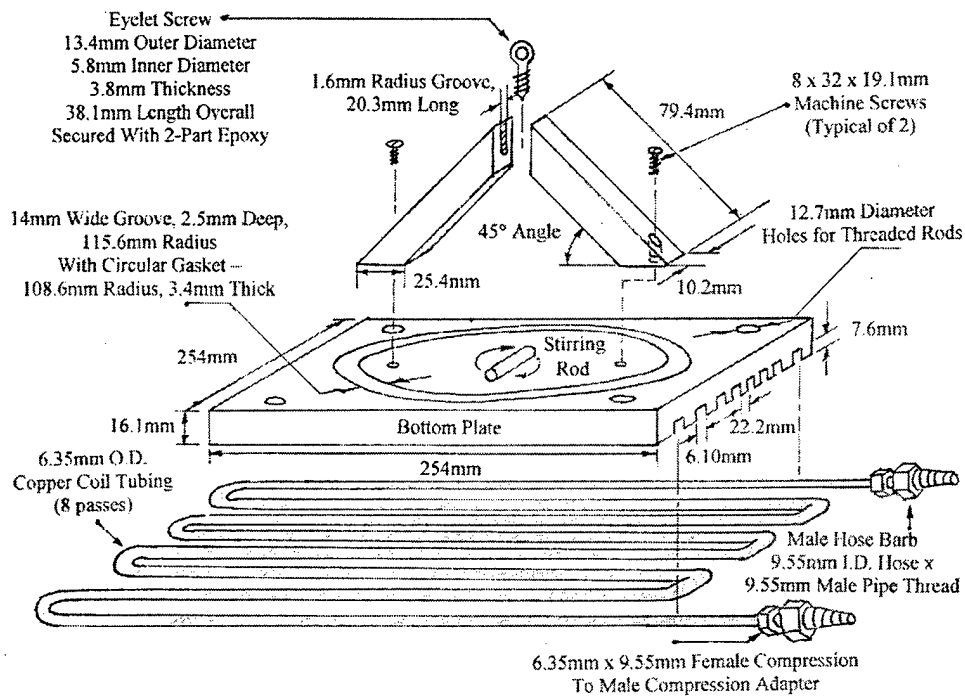


Figure 6: Bottom plate and bottom wire attachment point.

The bottom wire attachment point for the SMA wire sample assembly is comprised of three main parts: two aluminum beams machined to stand at 45° to the bottom plate's upper surface mate together at their apex to hold an eye screw in a machined groove. Two-part epoxy holds the two beams and the eye screw in place at the apex. The beams are fastened to the upper surface of the bottom plate with a machine screw on each leg. For a maximum anticipated mass application of 2,000g to the SMA wire, the dimensions of the bottom support and solid connection to the bottom plate indicate that displacement or temperature-induced dimension changes of this support would be negligible. The bottom attachment

point serves as both a solid connection point for the SMA wire assembly, and permits a plastic coated stirring rod to spin in the center of the plate at varying speeds under magnetic input from the supporting hot plate. The aluminum bottom plate permitted the magnetic influence of the hot plate to spin the stirring rod without significant interference.

Top Plate

The top plate was penetrated by six each 7.5mm diameter holes for various fittings used in previous experiments. For SMA experiments, a hole in the plate's center served as the access point for the wire assembly to exit the environmental container and attach to the weight application lever. A second hole supported the digital temperature controller for the hot plate. A third hole supported the analog mercury glass thermometer. The remaining three pre-existing holes were left open with no obstructions to allow some heat to escape the environmental container and prevent unnecessary interior air pressure buildup. To permit accelerated heating, one additional 10mm diameter hole was machined in the top plate at the location of the insulated heat pipe discharge. The top plate served as the point of attachment for the weight application lever fulcrum, tensioning crossbar, and support for the insulated heat pipe that guided the heat gun's air flow.

Plastic Cylinder

The two aluminum plates are separated by a 300mm long, 231mm outer diameter cast acrylic cylinder with 14mm thick walls. This cylinder provided the

advantage of observing both the SMA wire sample assembly and the mercury filled glass thermometer during the course of experiments.

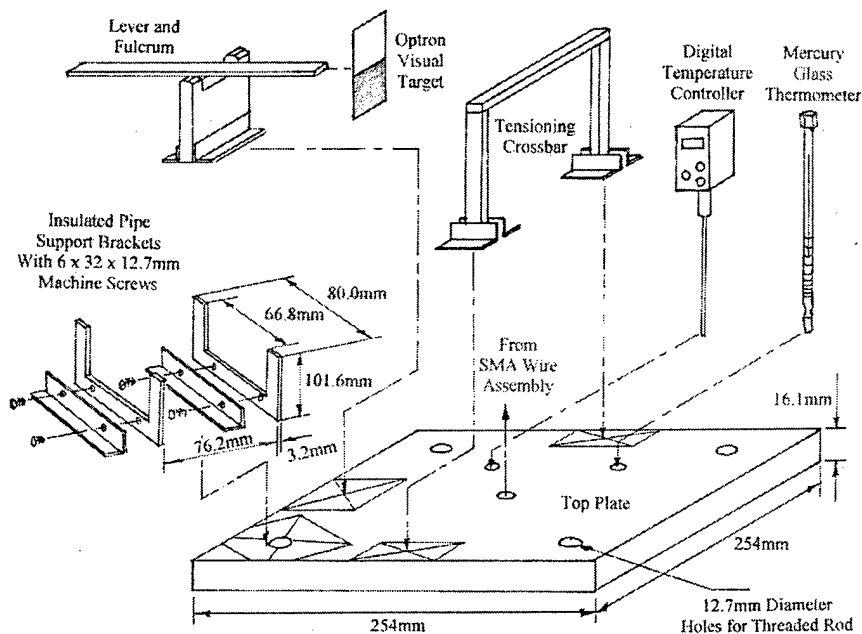


Figure 7: Top plate with attachments.

Hot Plate

A Corning™ model PC-420 hot plate provided the support surface for the environmental chamber, heat input for the bottom plate, and stirring impulse for a plastic-coated stirring rod located inside the environmental chamber. The rod spin rate varied from 0 at the hot plate's '0' setting to 150 rpm at the '10' setting, with experiments conducted at the '8' setting for a stir rate of approximately 120 rpm. Temperature control was provided by a combination digital temperature sensor and control element with 250mm stainless steel immersion probe.

Heat Gun

A Steinel model HL 1502S Hot Air Gun provided the heat source for the environmental chamber's top plate. The heat gun was set up vertically on a small wood stand so that the hot air output would directly enter a 32mm insulated steel heat pipe as shown in Figure 8. The heat pipe was wrapped in aluminized ceramic fiber insulation and channeled the hot air output from the heat gun to the top plate. Two small brackets clamped to the top plate supported the heat pipe as shown in Figures 7 and 8.

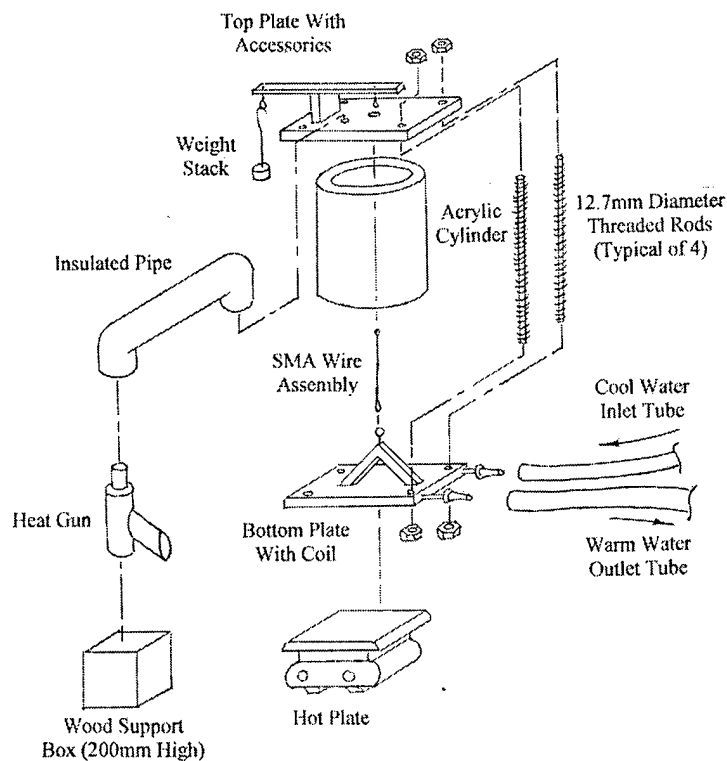


Figure 8: Environmental chamber exploded view.

Thermometer

A general purpose total immersion mercury glass thermometer with a temperature scale of -20°C to +120°C in gradations of 1°C provided the second temperature measurement for experiments.

DISPLACEMENT MEASUREMENT

Assuming effective lengths of SMA wire samples in the environmental chamber of 90.0mm, maximum anticipated length deflections would approach 9.0 mm. Applied masses would generally measure under 1000 grams for temperature-cycling tests, so a measuring device that did not touch the wire or its supports (and thereby influence readings) was desired. Two types of sensors were used to measure SMA wire displacement: an electron scanning device of trade name Optron™, and a displacement transducer.

Optron™

The Model 561 Electro-Optical Biaxial Tracking System (or "Optron") was an electro-optical displacement follower designed to track the motion of a target along vertical or horizontal axes. Sensing was performed without contacting the specimen, which made it attractive for planned Shape Memory Alloy experiments. To measure displacement of a body, a visual target like the one shown in Figure 7 was made with a solid black portion and a solid white portion with a clear line between the two areas. The target was fastened directly to the body and moved with it. The Optron Optical Tracking Head was mounted on a fixed surface and detected movement in the body's target.

The Optical Tracking Head locked on to a sharp discontinuity in the intensity of light reflected at a light-dark interface and focused it onto the photo cathode of an image dissector tube. Electrons were emitted from the back side of the photo cathode and accelerated to refocus on an aperture hole. When a target experienced displacement, the quantity of electrons entering the aperture hole changed, and the device compensated by creating a magnetic field to deflect the electron beam back to its original position. The voltage needed for this deflection was directly proportional to the displacement of the target, and this voltage was sensed and displayed by a connected oscilloscope. The ratio of target displacement to output voltage was essentially linear over the device's full scale measurement range.

The Optical Tracking Head was designed to stay in a fixed position relative to its target, and for each particular application, fixed lens extenders changed the focal length of a single focus lens to create sharp internal image. Following the manufacturer's guidance, lens calculations were performed to determine working distance and the length of the lens extension barrel required as described in Appendix B. To compliment these focusing calculations, the Optical Tracking Head was physically displaced forward and back from the target using the recommended lens barrel until a sharp focus developed in the sighting lens. The distance from lens to target was measured and compared favorably to calculated values.

For best performance, the target itself must be illuminated from the front by a direct current light source, or the Optical Tracking Head may detect the 60

cycle change in light intensity from overhead fluorescent lights and skew results by attempting to track apparent optical motion. The target should be a sharp contrast of flat (non-gloss) black and white color that completely fills the sighting lens and is oriented perpendicular to the optical axis. For these experiments, a standard white 3"x5" index card was oriented vertically and colored black on the bottom half to create a sharp black and white interface. The card was then attached to the end of the weight application lever with clear adhesive tape.

The Optron kit came with a control unit that housed all gain and sensor controls to provide power and control for the Model 806 Optical Tracking Head that sensed light inputs. (23)

Oscilloscope

A Hewlett-Packard Model 54600A oscilloscope provided displacement voltage outputs for all experiments. The oscilloscope was adjusted to receive and display a single voltage source input from either the Optron or the displacement transducer.

Displacement Transducer

A Hewlett Packard model 7DCDT-1000(FU) displacement transducer with a standard core provided an alternate method to measure SMA wire displacement. The displacement transducer operated by receiving a DC electrical input from a DC power supply, converting DC to AC to excite a primary solid-state winding, and measuring voltage induced in a secondary winding as influenced by the relative position of a standard sliding core. The standard core was a 3.05mm diameter stainless steel rod that made a sliding fit when inserted

into the coil so that the coil is essentially a sliding bearing, with the bottom of the core resting on the weight end of the weight application lever and thus indirectly measuring the displacement of the SMA wire. Calculations in Appendix B describe the conversion of transducer signal to SMA wire displacement. Before use, the transducer was calibrated and the calibration curve for the transducer is shown in Appendix B. (24)

Displacement Transducer DC Power Source

The displacement transducer required a DC electrical power source. A 120VAC model manufactured by Harrison Laboratories was used for experiments and wired as shown in Figure 10.

TESTING CONFIGURATIONS

The environmental chamber setup, heating, cooling, weight application, temperature measurement, and voltage measurement methods remained the same for all experiments. Use of either the Optron optical measurement device (Figure 9) or the displacement transducer (Figure 10) changed the measurement method that bridged the gap between SMA wire displacement and the voltage output at the oscilloscope. Since the SMA wire sample was wholly contained within the environmental chamber, SMA wire length change was measured indirectly by sensing displacement of the weight application lever either optically through use of the Optron™, or by physical contact of the displacement transducer's core with the top of the weight application lever.

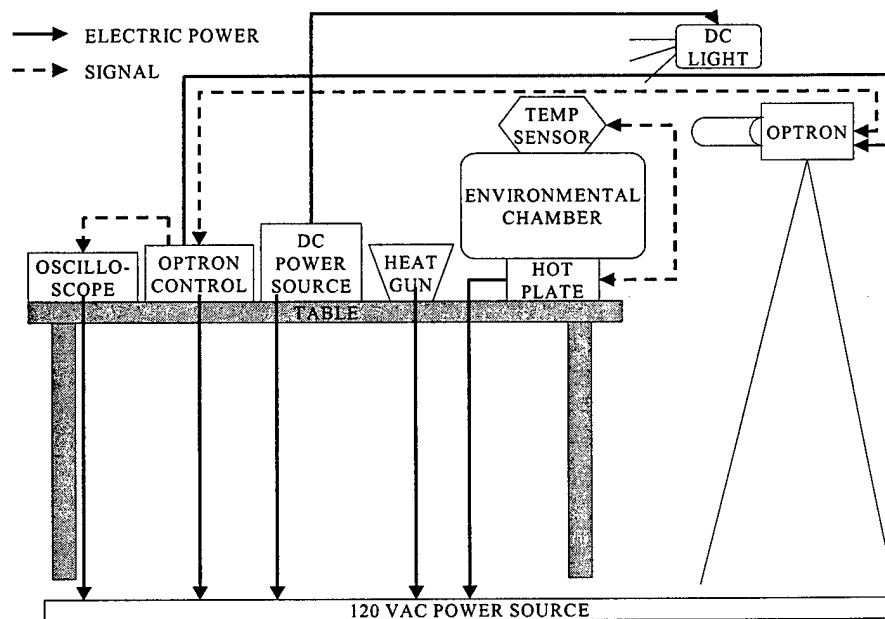


Figure 9: Wiring configuration for measurements with Optron™.

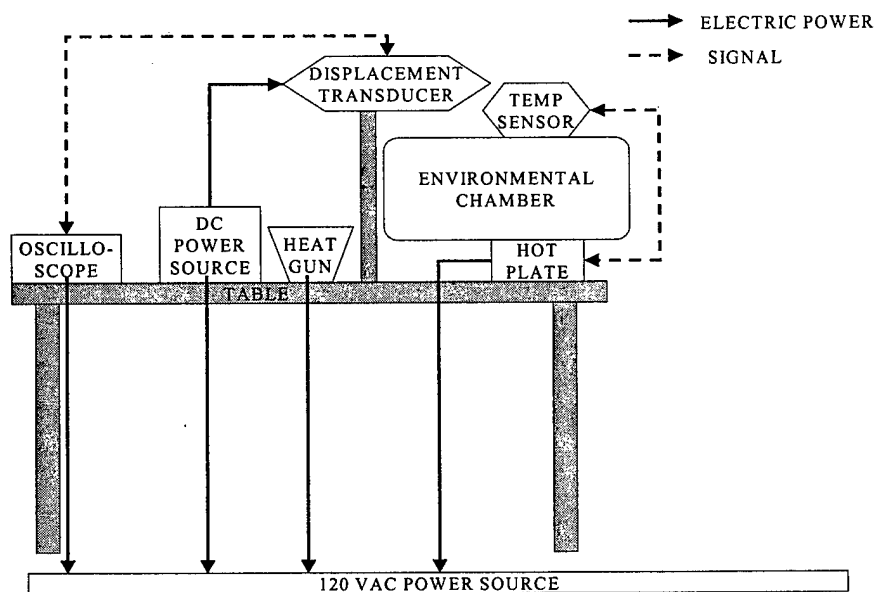


Figure 10: Wiring configuration for measurements with displacement transducer.

Chapter 3: Experimental Design: *Statement of the Problem*

Shape Memory Alloy actuators in the form of wires procured from a manufacturer must be tested to verify physical properties and performance prior to use in an operational mechanical design. Data on transition temperatures, electrical resistance, recovery force and other properties accompany SMA wires procured from the manufacturer. However, since properties are highly dependant on the mix of alloying elements and the stress state of the actuator, departures from manufacturer data are to be expected. The amount of departure from specified parameters may have a significant impact on load capacity, shape recoverability or energy consumption. To ensure the performance of SMA actuators does not adversely affect operation in intended applications, experiments are required to define properties as accurately as possible to permit safe and practical use.

Experiments will verify that the apparatus is capable of creating inputs and detecting outputs to a reliable accuracy. Experiments will also verify that the SMA samples actually do undergo a hysteresis cycle, and should be able to detect asymmetry within the hysteresis curve itself. The repeatability of runs will demonstrate that proper loads were selected and that the wires will cycle with approximately the same response, meaning that experimental data can be relied on to predict how the actuator will respond in different temperature envelopes and loading configurations.

SPECIFIC VARIABLES TO BE MEASURED

The geometry of a planned underwater propulsion system could be significantly impacted by the contraction length of the SMA actuators, so length change will be measured as a dependent variable in response to loading inputs. Length of contraction is also the primary indicator of the status of phase transformation of the material from austenite to martensite. Length will be measured through use of either the Optron™ Optical Measurement System or the displacement transducer, both of which produce an output to an oscilloscope measured in volts.

Concurrent with measurements for displacement, measurements of temperature were taken through use of a digital temperature controller that controls the electric hot plate, along with a mercury glass thermometer. The digital temperature was the primary trigger for taking readings of the glass thermometer, voltage at the oscilloscope output, and elapsed time of the experiment.

Prior to insertion of the SMA wire assembly into the environmental chamber, a measurement of its effective length was taken using a standard micrometer. This initial length served as the basis for strain calculations. Diameter of the wire was also measured with the micrometer and verified against the manufacturer's information.

The masses used for application of force to the weight application lever were verified prior to application on the weight stack.

If the displacement transducer was used as the measurement device, the distance from the contact point of the transducer's core to the fulcrum of the weight application lever was used to convert transducer displacement to sample displacement. Similarly, calibration of the Optron™ Optical Measurement Device and measurement of the distance between the optical target and the point of connection of the SMA wire allowed corrections to voltage outputs. Measurement of the distance between the Optron™ lens and the optical target verified that the optical mechanism was optimally placed for obtaining readings.

SELECTION OF FACTORS TO BE VARIED

Heat content was chosen as an independent variable and was cycled from at least 10°C below the manufacturer's listed martensite start temperature to at least 10°C above the listed austenite finish temperature to completely encompass a full hysteresis cycle. Heat input was provided by an electric hot plate and a heat gun, with either one heating unit or both functioning, depending on the rate of heat input desired.

The amount of mass applied to the specimen through the weight application lever was also independently varied, with expected dependent variables being the stress level in the wire, wire length, and, indirectly, transition temperatures, Young's Modulus, and other properties.

Since the manufacturer provided SMA wires of similar composition in seven different diameters, diameter of the SMA wire was varied in separate experiments. The manufacturer provided SMA wires in both a low temperature (LT) and high temperature (HT) alloy compositions, so the alloy composition was

also varied in separate experiments. Manufacturer data for the Low Temperature Series indicated that a fully hysteresis cycle would begin at 42°C and complete at 68°C, while the High Temperature Series transitioned through a hysteresis curve 20°C higher, between 62°C and 88°C. Predicted annealing temperatures of 300°C and a melting temperature of 1300°C indicated that exposures to temperatures under a planned experimental value of 110°C would not adversely affect the SMA samples.

Although not specifically factors, the measurement devices were changed from the Optron™ to the displacement transducer to verify functionality of the apparatus and determine the advantages and limits of each method of measurement.

CHOICE OF FACTOR LEVELS

By applying mass to the apparatus, the stress level in the wire changes proportionally. For each diameter of wire, manufacturer supplied data included three sets of data on recovery force as a function of stress level. The manufacturer's data for "Maximum Recovery Force at 600MPa" that the wire can exert was an indicator of how much mass can be applied to the sample without inducing plastic deformation that the wire could not recover. "Recovery Force at 190MPa" indicated an 'average' stress level that would permit full cycling of the wire, but without returning to its original unloaded length during testing. "Recovery Deformation Force at 35MPa" indicated the minimum amount of mass to apply to the lever to allow the wire sample to cycle completely through the hysteresis and return to a length close to its original length. Loading at less than

the 'recovery deformation level' would allow the SMA sample to complete a reverse transition from martensite to austenite, but the sample would not have sufficient impetus to be stretched back out to its originally 'deformed' martensitic length and the hysteresis curve would not completely close. Variance of the mass was to be quantitative with planned sequences of loading and unloading. Increments of applied mass were to be varied between 0.5g and 100.0g to test the responsiveness of the sample and measuring apparatus. Since the manufacturer did not indicate at what temperature the above described stress levels were valid for, the conservative assumption was made that manufacturer provided data were valid for room-level temperatures of 25°C – 30°C. Experiments were planned to be conducted for cycling of mass amounts at different ambient temperatures, to determine the effect of temperature on load capacity of the alloys.

Temperature was to be varied and measured at each degree change as indicated on the digital thermometer, along with other output variables as listed above. During periods of very slow temperature change, the mercury glass thermometer was planned to be read at each change of degree or half degree Celsius as the impetus for obtaining a full set of readings.

DEFINITION OF THE INFERENCE SPACE FOR THE PROBLEM

The limits on the inferences drawn from experimental results will be directly affected by the measured or anticipated value of error for each measurement. Accuracy levels for devices as obtained from manufacturer references include:

- Thermometers: $\pm 1.0^{\circ}\text{C}$

- Variability induced by separation of thermometers and temperature variance within the environmental chamber: $\pm 1.5^{\circ}\text{C}$
- Oscilloscope: $\pm 20\text{mV}$ (per manufacturer data)
- OptronTM: $\pm 20\text{mV}$ output
- Micrometer measurements: $\pm 0.005\text{in}$ or $\pm 5.0\mu\text{m}$
- Masses: ± 0.1 grams

Based on these errors, accuracy on measurement length of SMA wire samples should approach $\pm 8.0\mu\text{m}$. Since measurement of the transition temperatures occurred in nonlinear areas of the hysteresis curve, overall transition temperature accuracy was forecast as $\pm 3.0^{\circ}\text{C}$.

NUMBER OF SAMPLES TO BE TAKEN

The number of SMA wire samples experimented upon was limited only by time available to complete experiments. Improving the accuracy and controllability of the experimental apparatus consumed most of the project effort. Fifteen partial or full experimental runs were conducted with the purpose of improving the testing system and, once reliability was established, usable experimental data was finally obtained. Three experiments of differing types were completed and are analyzed in Chapter 5.

NUMBER OF OBSERVATIONS TO BE TAKEN

With temperature as the primary input during heat cycling experiments, observations were taken at each change of degree Celsius on the digital thermometer. Observations taken for each changing degree included indicated

temperature of the glass thermometer, voltage output of the oscilloscope, and elapsed time for the experiment.

For weight application experiments, full cycle weight experiments were conducted at a quasi-stationary temperature and observations were taken at each addition or removal of a mass to the weight application lever. Manual control of temperatures in the environmental chamber was possible within $\pm 3.0^{\circ}\text{C}$ for extended periods after practice with the hot plate and heat gun inputs. Temperatures of the digital and glass thermometers were recorded along with the voltage output of the oscilloscope for each applied mass.

After the addition of mass increments ≥ 20.0 grams, 45 – 60 seconds of time were allowed to elapse to permit output voltage readings to stabilize, indicating that the wire had attained its fully displaced length for that particular mass input.

ORDER OF EXPERIMENTATION

To ensure a random nature of the experiments and provide meaningful feedback for evolving the heating and cooling mechanisms testing apparatus, experiments were carried out after randomly selecting the diameter of wire to undergo testing. Also, testing on the low temperature alloy series of wires was performed in a random mix with high temperature alloy series.

Weight experiments were carried out at the start, middle, or end of a thermal cycle. Completely heating the alloy sample to above the austenite finish temperature ensured that the material was transformed completely to austenite,

recovering and residual strain and returning to its original dimensions before application of weight commenced.

HYPOTHESES TO BE TESTED

Five hypotheses to be tested were:

- The SMA wire will completely transition through a hysteresis curve at transition temperatures listed in manufacturer literature when exposed to a consistently varied thermal environment.
- The SMA wire will displace in response to varying applied forces and will exhibit elastic deformation that is partially recovered when the force is removed.
- The SMA wire will exhibit varying values for Young's Modulus, dependent on the temperature selected for the experiment.
- The remainder of elastic deformation can be regained when the SMA wire sample is heated through the austenite finish temperature and then cooled.
- If loaded with masses greater than manufacturer recommendations, the SMA wire will exhibit plastic deformation that cannot be recovered through thermal cycling.

Chapter 4: Experiments: *Procedures and Sequence of Operations*

A total of three experiments were conducted, and within each experiment were several different runs. Experimental runs were of two distinct types that focused on either length change in response to temperature input or length change in response to load input.

To conduct a full cycle test, calibration of the measurement device for the test was performed as described in Appendix B to ensure accurate output correlations were obtained for that particular experiment. The experiments were conducted within easy reach of a water supply and drain, along with at least four 120VAC electric 2-prong outlets. The environmental chamber was set above the hot plate and was located on the same table as other measuring devices, except for the Optron which was on its own tripod. An SMA wire sample was selected and the wire assembly was constructed to dimensions shown in Figure 3 in Chapter 2. The environmental chamber top plate was removed and the wire assembly was connected to the bottom connection point in the environmental chamber, threaded through the center hole in the top plate, and connected to the weight application lever. The bolts holding the top plate in place were then securely tightened. Tare mass was selected and then applied to the opposite lever end to stretch the SMA wire sample assembly taut and remove as much slack as possible from the experimental apparatus. The Optron or displacement transducer were connected to the oscilloscope and initial readings are taken for temperatures and voltage

outputs. The heat gun was placed on a small wood stand so its output nozzle was oriented directly into the insulated heat pipe. See Figures 9 and 10 for example experimental setups.

For a thermal cycling experiment under constant load, the hot plate temperature was set to a value of 8 or 10 on a scale of 0-10, the stirring rod was set at a speed of 8 on a scale of 0-10, and the heat gun was set on 800°F, all of which were switched on at the same time. Temperatures were allowed to increase unimpeded, and measurements were taken based on each degree change of the digital temperature controller. At each temperature reading, average voltage as indicated by the oscilloscope was recorded, along with the time of the reading. Intermediate temperature readings were taken where temperature change was slow, particularly during the first 10 minutes of heating, when changing from heating to cooling, and at the end of the cooling cycle. After reaching peak temperatures at least 10°C above the manufacturer's listed maximum transition temperature, the heat gun was removed from its position and relocated so that it could cool with its fan on per manufacturer recommendations. If the heat gun were allowed to cool while still connected to the heat pipe, air movement from the heat gun would pick up a significant amount of convected and radiated heat from the interior of the pipe, and would therefore impede cooling of the top plate.

To begin cooling, water was slowly added to a single rubber tube at one end of the cooling coil by allowing water to drip into the tube and flash to steam. Depending on the rate of water addition, cooling water input to the cooling coil was repeatedly ejected by expanding steam, until no more steam was formed upon

addition of water. Cooling proceeded slowly until no more steam was formed at a sample temperature of 85°C, and then the rubber cooling tube was then connected directly to faucet input. Cooling then proceeded exponentially with steady water flow, and peak temperature change rates approached 3°C per minute. Cooling proceeded until indicated temperatures were within 5°C of room temperature. See Appendix C for representative apparatus heating and cooling rates.

GENERAL OBSERVATIONS

During heating, the rising temperature of the digital thermometer (which was in contact with the top plate through a metal coupling fitting) led the temperature of the glass thermometer. During cooling, the temperature of the glass thermometer was first to decrease, affording to its proximity to the bottom plate which underwent active cooling. These differences in reaction time to temperature variance were a reason to use two thermometers that sensed environmental chamber temperatures at different locations, and to take their averages as representative chamber and SMA wire temperatures.

During rapid temperature changes, two experimenters improve accuracy of measurement, since four readings from different locations are taken at almost the same time: two temperature readings from the environmental chamber, a voltage reading from the oscilloscope, and a time reading. Slowing the rate of temperature change or developing an automated data acquisition scheme would eliminate the requirement for the second experimenter.

DIFFICULTIES ENCOUNTERED AND THEIR RESOLUTION

A major objective in the project was to develop a reliable testing device that would conduct full-cycle tests in a reasonable amount of time. The apparatus needed to increase and decrease sample temperature while monitoring the SMA wire's state during the process.

Given that the manufacturer's literature stated that upper transition temperatures were as high as 98°C, the apparatus needed to be capable of exceeding that upper limit by approximately 10% to encompass a full temperature transition cycle. The additional 10% would take into account that the wire may undergo transitions at different temperatures due to production variances or due to stress induced as part of the experiment. The hot plate alone on the bottom surface of the environmental chamber was capable of heating the wire to 85°C, 25°C short of the required temperature of 110°C. The heat gun and associated piping and insulation were added to heat the chamber's top plate, and with input from the heat gun on the 800°F setting, the chamber became capable of easily exceeding 110°C.

Solution of the heating problem caused another problem: after rapid heating, the chamber absorbed a significant amount of heat in the top and bottom plates and connecting steel rods. Without a method to force cool the chamber, sample cooling would take over three hours. Assuming water as a cooling medium, the cooling method had to be self contained, could not lead water, could not use air currents that would disturb the paper target on the end of the weight application lever, and could not change the elevation of the environmental

chamber in relation to the Optron measuring device during thermal cycling, or readings would be skewed.

Metal pans of 16GA galvanized roofing sheet steel and 18GA sheet aluminum were fabricated and positioned between the hot plate and the lower surface of the bottom plate to allow outside input of water to flow around the outside of the bottom plate, and then to drain the water after heating as shown in Figure 11.

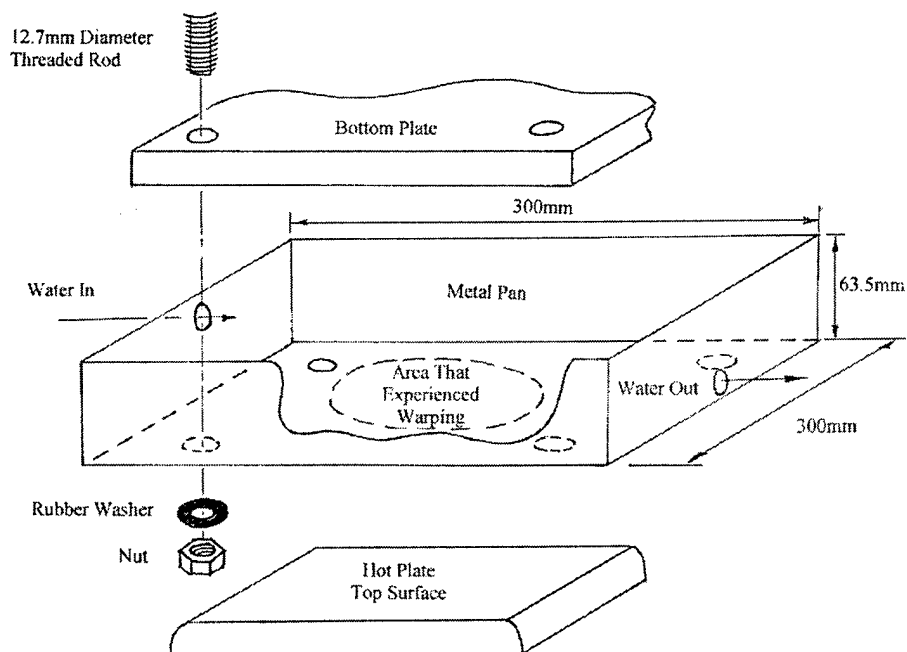


Figure 11: The concept of the failed cooling pan idea.

Four holes in the base of the pan allowed the pan to be fastened to the underside of the bottom plate with the four bolts serving as anchoring points. Eight machined grooves in the bottom plate allowed water to circulate between the pan and the center area of the plate, where the majority of heat originated.

The heat generated by the hot plate significantly increased the temperature of the center of the pan relative to the pan's outer edges, and after reaching 65°C, the pan spontaneously bowed in the vertical plane approximately 3.5mm and caused lifting of the entire environmental chamber off the surface of the hot plate, invalidating wire displacement readings. A third test of a Teflon-coated baking pan with no holes drilled and without the environmental chamber's weight placed on top revealed the same problem: the high heat rate provided by the hot plate in a small area of the pan caused differential expansion of metal and resulted in bowing and warping of the center area of the pan relative to its borders.

The steel pan presented another, unexpected hurdle. With the steel pan placed between the fully assembled environmental chamber and the hot plate, the metal stirring rod could no longer spin under the influence of the hot plate, owing to magnetic interference caused by the steel. Therefore, all metal between the hot plate and its stirring rod had to be non-magnetic.

To eliminate the vertical displacement caused by using an intervening pan, the machined grooves in the bottom plate were widened to accept thin wall copper tubing, which was forced into these grooves and carried water to cool the bottom plate. The heating cycle of the experiments occurs without water inside the copper cooling tubes. At indicated environmental chamber temperatures above 85°C, the bottom metal plate's temperature was still near 100°C, and water flashed to steam when first introduced into the rubber cooling tubes, causing water introduced into the system to be pushed back out the input tube by expanding steam. The rubber cooling tube could not be connected directly to a

faucet until all steam flashing has ceased, or the steam's pressure might have ruptured cooling system components. High temperature heater hose was required to sustain temperatures at the boiling point without melting the hose material.

While using the Optron, the target indicator had to be illuminated by a closely positioned DC light source, or overhead fluorescent lights operating at 60Hz increased interference as the DC light is moved away from the target. At a target-to-DC light source distance under 300mm, the amount of overhead light interference appeared minimized. A good portion of the Optron's internally generated signal sensing noise was due to the high voltage supply needed for the photo tube to operate, although the amount of noise is not quantified by the manufacturer. Stopping down the single focus lens helped improve the signal to noise ratio. An experiment was conducted to quantify the 'drift' of the Optron's voltage output over a period of time, and is presented in Appendix B.

While conducting weight cycling tests, loads exceeding 600g approached the holding strength of the mechanical crimps that held the thin SMA wires in place. To conduct tests using greater masses, a method to couple very thin wires to supporting steel wires will have to be found.

An initial test with the displacement transducer connected to the tensioning crossbar directly above the SMA wire verified the manufacturer's recommendation that the device not be used in applications over 140°F. Heat from the top plate and heat gun rose to the transducer, causing erratic readings. The transducer was recalibrated and moved to the weight end of the weight

application lever and separately supported to avoid thermal input from the environmental chamber.

OPERATIONS CONDUCTED IN INDIVIDUAL EXPERIMENTS:

Experiment #1

For Experiment #1, a sample of 150LT Muscle Wire with a tare load of 49.7 grams was set up in the environmental chamber as described in Chapter 2. Displacement measurement was provided by the Optron™ Optical Measuring Device as shown in Figure 9.

For Experiment #1 Run #1, at a constant temperature of 23°C as indicated by the mercury glass thermometer, with 49.7 grams tare mass, masses of increment 0.5 grams were added to the tare mass until reaching a total of 54.7 grams. After applying all desired mass, all mass above the tare mass was removed at once to return to a loading of 49.7 grams on the weight application lever. No heat was added during this portion of the experiment, and the hot plate's stirring rod was not activated.

For Experiment #1 Run #2, only the hot plate provided heat to the bottom plate. Starting at room temperature of 23°C, the hot plate heating element was energized and set at level 10, with the stirring rod rotating at a commanded speed of 8 of 10 from the speed scale. Temperature was allowed to increase to an indicated temperature of 80°C on the digital thermometer before heat was turned off. Readings were manually recorded at each degree of digital temperature change. The stirring rod remained energized at constant speed until completion of the experiment. Temperature inside the environmental chamber continued to

climb and eventually stabilized at 84°C, and then cooling proceeded by natural convection and radiation. The duration of cooling from 84°C to 27.5°C exceeded 3 hours for this portion of experiment, and this slow cooling rate served as the stimulus for developing an efficient cooling system that would drastically reduce cooling time.

Experiment #1 Run #3 occurred in the middle of Run #2, at the peak of the temperature curve at 84°C. Masses of 20 gram increments were added to the tare mass until total mass reached 189.7 grams, and were then removed individually to return to the tare mass of 49.7 grams.

Experiment #2

For Experiment #2, a sample of 150HT Muscle Wire with a tare mass of 49.7 grams was set up in the environmental chamber as described in Chapter 2. Displacement measurement was provided by the Optron™ Optical Measuring Device as shown in Figure 9.

For Experiment #2 Run #1, at a constant temperature of 23°C as indicated on the mercury glass thermometer, with 49.7 grams tare mass, masses of increment 0.5 grams were added to the tare mass until reaching a total of 54.5 grams, after which each mass was then individually removed until returning to the tare loading of 49.7 grams on the weight application lever. No heat was added during this portion of the experiment, and the hot plate's stirring rod was not activated.

For Experiment #2 Run #2, heating was provided by both the heat gun and hot plate, which were energized together at the start of the run. The heat gun was

set at a temperature of 800°F and the hot plate was set to a heat level of 8 of 10, with its stirring rod spinning at a commanded speed of 8 of 10. At a temperature of 102°C, the heat gun was removed from the heat inlet pipe, the hot plate heating element was turned off, and the hot plate stirring rod continued at a commanded speed of 8. Cooling water was gradually added to the cooling coil until steam no longer flashed at an indicated environmental chamber temperature of 85°C, at which point the cooling hose was connected directly to a faucet and a steady stream of cooling water was applied until reducing the environmental chamber's temperature to 62°C. At this point, Experiment #2 Run #3 was conducted. After completing Experiment #2 Run #3, cooling was resumed until reaching a temperature of 38°C.

Experiment #2 Run #3 was conducted at a mean temperature of 55°C. Masses of 20 gram increments were sequentially added and removed, increasing applied mass from 49.7 grams to 149.7 grams, and finally returning back to the tare mass.

Experiment #2 Run #4 began at the conclusion of Run #2, by once again adding heat to the environmental chamber starting at a cooled temperature of 37°C at the conclusion of Run #2. The hot plate heating element was energized to level 10 and the stirring rod remained energized at speed 8. The heat gun was not used to provide heat in this portion of the experiment.

Experiment #3

For Experiment #3, a sample of 250LT Muscle Wire with a tare load of 49.7 grams was set up in the environmental chamber as described in Chapter 2.

Displacement measurement was provided by the displacement transducer as shown in Figure 10.

For Experiment #3 Run #1, starting at a constant temperature of 45°C as indicated on the mercury glass thermometer, heat was added by energizing the heat gun to 800°F and the hot plate heating element was energized to level 10, with the stirring rod turning at speed 8. The temperature inside the environmental chamber was allowed to climb to a digitally indicated temperature of 70°C, at which point the heat gun was removed from the insulated heat pipe and the hot plate heating element was turned off. The hot plate stirring element remained energized at a speed of 8 through the remainder of the experiment's runs. Experiment #3 Run #2 was conducted at this point, while the environmental chamber possessed the maximum heat for the run. After completing Run #2, cooling water was added to the cooling coil, and a steady stream of tap cooling water was applied until the chamber reached a cooled temperature of 29°C.

Experiment #3 Run #2 was conducted at a mean temperature of 74°C, with masses sequentially added and removed on top of the tare mass of 28.3 grams.

Experiment #3 Run #3 was conducted at a mean temperature of 30°C similar to the sequence described for Experiment #3 Run #2.

Experiment #3 Run #4 conducted another heating cycle by starting at a digitally indicated temperature of 29°C and adding heat only with the hot plate's heating element set at level 10. Temperature climbed to 78°C on the digital thermometer, the heat input was turned off, and cooling water was applied to the cooling coil. Temperature continued to climb to 80°C before dropping under the

influence of cooling to 56°C. Cooling water input was stopped at this point, and Experiment #3 Run #5 commenced.

Experiment #3 Run #5 sequentially added masses in 50 gram and 100 gram increments, after which the masses were removed in the reverse sequence of addition until returning a tare mass of 28.3 grams. Masses were again added in 20 gram, 50 gram, and 100 gram increments until the upper crimping connection holding the SMA sample wire to the steel leader wire permitted separation at a total applied mass of 648.3 grams. The experiment was stopped at this point due to sample assembly failure, and all heat input and measuring devices were turned off.

Chapter 5: Analysis: *Introduction*

This Chapter presents a summation of data obtained from experiments. The interpretation of results is based on the hypotheses to be tested as listed at the end of Chapter 3. Graphic results of each experimental run and an experimental results summary table are shown in Appendix C.

DATA COLLECTION AND PROCESSING

The general procedure for each experimental run was followed as described in Chapter 4, with data recorded manually and then transferred to a spreadsheet program. Data recorded in millivolts was converted to wire length by using the calibration factors calculated in Appendix B. Indicated temperatures of the digital and mercury glass thermometers were combined into average temperature and used as an independent variable.

Plots for experimental runs varying temperature at constant load resulted in hysteresis curves with temperature as the abscissa and wire length as the ordinate. Data obtained from these graphs included start and finish temperatures for martensite and austenite, which were compared to manufacturer values.

Experimental runs varying load at constant temperature resulted in stress – strain curves with strain as the abscissa and stress as the ordinate. The slope of the lines was then calculated as Young's Modulus, which was also compared to the manufacturer's given data.

INTERPRETATION OF RESULTS: Hysteresis Curve

We begin by discussing the hypothesis "The SMA wire will completely transition through a hysteresis curve at transition temperatures listed in manufacturer literature when exposed to a consistently varied thermal environment." The experiments conducted developed anticipated hysteretic curves as shown in Appendix C, and therefore validate this hypothesis with conditions as noted below.

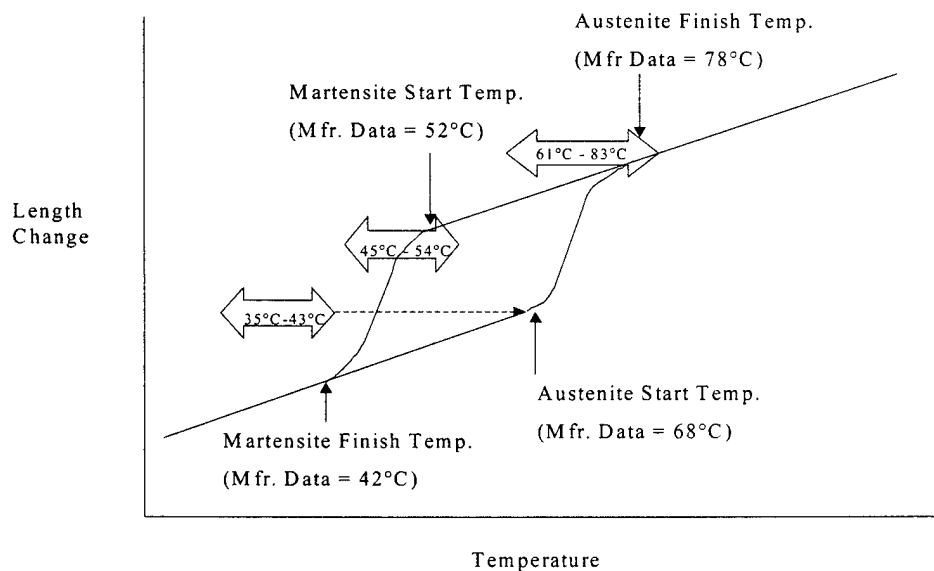


Figure 12: Experimentally obtained transition temperatures for Low Temperature series SMA wires are compared to manufacturer provided data.

Figure 12 shows how experimentally obtained transition temperatures compare to manufacturer data for the 'Low Temperature' (LT) series of Muscle Wires. Small vertical arrows indicate locations of manufacturer predicted

transition temperatures. The block arrows containing data indicate ranges of temperatures obtained from actual experiments. The location and length of the block arrows relative to the indicated manufacturer points depict the relative displacement and ranges of temperatures obtained experimentally. Figure 13 shows similar data obtained from the High Temperature (HT) series of wires.

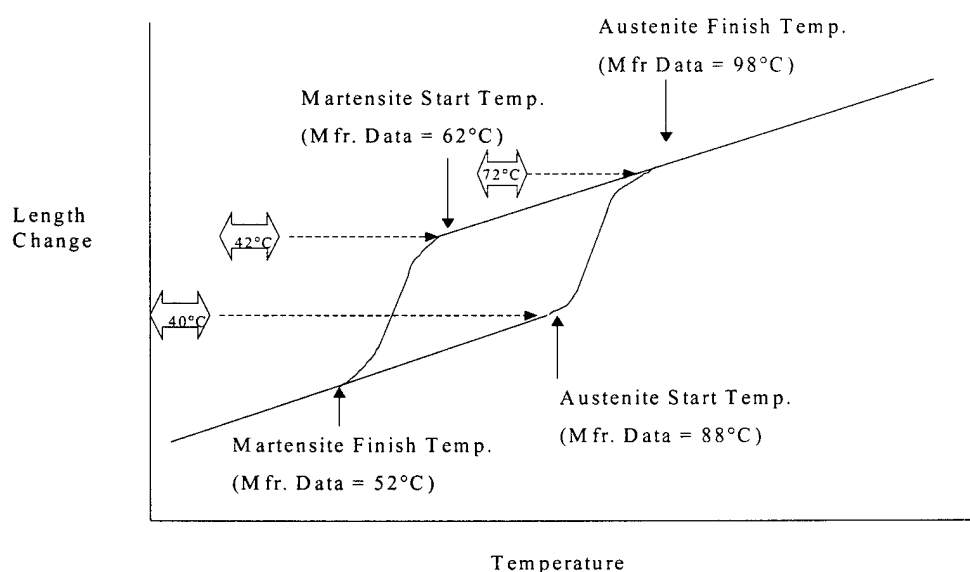


Figure 13: Experimentally obtained transition temperatures for High Temperature series SMA wires are compared to manufacturer provided data.

Clearly defined hysteresis curves were obtained experimentally the first time that the SMA sample wire experienced a heating and cooling cycle. After initial heat cycling, load application runs were conducted that changed the strain in the SMA wire samples. Subsequent attempts to thermally cycle wire samples after loading runs did not yield hysteresis curves with transition temperatures as

clearly defined. Observed SMA wire sample length changes through hysteresis cycles ranged from 0.83% to 4.68% contraction from initial length.

During a heating cycle, the LT SMA wires began forming austenite at austenite start temperatures 25°C – 48°C cooler than the manufacturer's predictions. The range of experimentally obtained temperatures for austenite finish correlated with manufacturer data, as did experimental temperatures for martensite start temperature. However, all experiments conducted were unable to obtain data for martensite finish temperature. After reviewing manufacturer literature and performing stress calculations, it became apparent that an error was made in calculating minimum tare mass for a complete hysteresis cycle. When the SMA wires were heated, they underwent predicted contraction while forming austenite. Since the wires were not acted upon by a sufficient force, they remained in the contracted state even as temperatures cooled to form martensite. Martensite start temperatures were detected, and hysteresis curves began their transition toward martensite finish temperature, but the curves failed to close even when samples were cooled below the predicted martensite finish temperature. Manufacturer provided data for "Recommended Deformation Force" indicate the minimum mass (in grams) that should be applied to a sample during cooling to permit complete cycling. For the 150 μ m wires, the 49.7 grams applied tare mass fell short of the manufacturer's recommended 62 grams, and so the SMA sample wire did not have sufficient impetus for re-stretching to its original length while cooling, and the hysteresis curve could not close. Proper calculation of force

required for complete SMA wire length recovery would have eliminated this problem and allowed detection of martensite finish temperatures.

Experimentally obtained transition temperatures for the High Temperature wire series were significantly below manufacturer values. Since increased stress on SMA actuators increases transition temperatures, and the SMA wire was loaded below the manufacturer recommended level, lower transition temperatures resulted. Since only one run was conducted with a High Temperature series SMA wire, additional replicates of experimental runs would be required to verify accuracy of the data and comment reliably on possible causes for the differences.

Elastic Behavior

We now consider the hypotheses “The SMA wire will displace in response to varying applied forces and will exhibit elastic deformation that is partially recovered when the force is removed” and “The SMA wire will exhibit varying values for Young’s Modulus, dependent on the temperature selected for the experiment.”

Tests were performed at quasi-static temperature ($\pm 3^{\circ}\text{C}$) and resulting Young’s Moduli are itemized in Table 1. Plots in Appendix C indicate that wires lengthen in response to load application, recover the majority of their stretched length when unloaded, and possess some residual strain at the conclusion of load application. Residual strains ranged from 0.01% to 5.97% of total length at the conclusion of loading experiments. As expected, higher applied forces resulted in higher wire strains.

Stress-strain plots in Appendix C indicate that essentially linear elastic behavior was observed while loading SMA wires. However, when unloaded, two distinct behaviors were noted. During the initial portion of unloading, the SMA wires exhibited essentially linear behavior. After removing approximately half the applied force, the SMA wire samples increased their rate of recovery to more closely approach the effective length at the start of the loading cycle, resulting in a smooth curve for the second half of unloading. Higher applied loads made this difference between linear and curvilinear sections more pronounced. Because slope was constant for the first part of the recovery and variable for the second part, values in Table 1 were calculated from the point of maximum strain to the final value of strain after all experimental loads were removed to represent the overall behavior from maximum to minimum strain state. Some residual strain was present in experimental runs, indicating that the SMA wires had temporarily deformed in length in response to loading, which indicated agreement with the elastic behavior hypotheses.

One experimental run (Experiment #2 Run #1) at low temperature indicated that the SMA wire sample experienced unexpected spontaneous recovery to a length shorter than its original length at the start of the weight application process. In the absence of heat stimulus to shorten the wire's length, possible causes for this anomaly include the presence of residual strain in the alloy resulting from the manufacturing process, or experimental noise.

Young's Modulus Analysis				
	Wire Type	Temperature (deg C)	Range of Mass Applied (g)	Young's Modulus (Gpa)
	150 LT	23	49.7 - 54.7	7.95
	150 LT	83	49.7 - 189.7	6.93
	150 HT	23	49.7 - 54.7	17.58
	150 HT	55	49.7 - 149.7	9.58
	250 LT	30	28.3 - 92.3	161.92
	250 LT	47	28.3 - 116.3	137.89
	250 LT	74	28.3 - 648.3	12.35
	Manufacturer Data:		Austenite	75
			Martensite	28

Table 1: Young's Modulus as determined through experiments compared to Manufacturer data (22).

Manufacturer data for Young's Modulus indicated a lower value for martensite and higher value for austenite, but no correlation of these values with varying temperature was provided. (22) Since it was not possible to determine the exact volumetric percentage of austenite and martensite in the SMA wire at a particular temperature, we would have to rely on the value of Young's Modulus to indicate a proportion of austenite to martensite corresponding to the value of Young's Modulus. Based on manufacturer data, Young's Modulus should have been at a low value of 28GPa corresponding to the wire's martensitic state at low temperature. As the wire sample's temperature increased, the value of Young's

Modulus should have approached a maximum value of 75GPa at the austenite finish temperature.

However, materials texts indicated that for common metals such as steel and copper, Young's modulus should decrease as temperature increases, owing to changes in intermolecular forces that cause the metal to lose the ability to absorb equivalent strains and still exhibit recovery. (25) Results in Table 1 indicate agreement with standard material theory, in that Young's Modulus decreases with increasing temperature for both the Low Temperature and High Temperature series of wires. Experimental values for Young's Modulus range from 7 to 162, greatly exceeding the range of manufacturer provided values.

Recovery of Strain with Heating

We now analyze the hypothesis: "The remainder of elastic deformation can be regained when the SMA wire sample is heated through the austenite finish temperature and then cooled." In each experiment set, runs varying temperature were conducted after load cycling runs to test this hypothesis. In each of four cases shown in Appendix C, the SMA wire samples recovered the residual strain from loading experiments and contracted further until reaching a final shortened length.

Loading Beyond Manufacturer Recommendations

We now consider the last hypothesis: "If loaded with masses greater than manufacturer recommendations, the SMA wire will exhibit plastic deformation that cannot be recovered through thermal cycling." Attempts to load the SMA wire past manufacturer recommendations revealed that the mechanically crimped

connections between the SMA wire and the supporting wire could not sustain forces exerted by heavy loads. The connection between the SMA Wire and its supporting wire will have to be improved before this hypothesis can be properly tested.

CONCLUSIONS AND RECOMMENDATIONS

This report studied the behavior of Shape Memory Alloys through development and execution of an experimental concept. An apparatus was constructed to meet experimental needs and then used to perform thermal cycling and load cycling tests on SMA wire actuators. Data were obtained and analyzed to validate the concepts for the experiments.

It was observed that the apparatus had the ability to detect transition temperatures and changes in length due to application of force to the wire actuators. The experimental apparatus performed well for detecting start and finish temperatures for austenite and martensite and in calculating Young's Modulus, with deviations from manufacturer literature as noted. Therefore, the concept employed in this report of applying heat and loading inputs to obtain displacement data appears valid. Areas for potential improvement of the experimental apparatus include:

- Use of a laser displacement detection device would increase accuracy while imparting no forces on the SMA wire.
- Use of automated data acquisition for output voltages and input temperatures would increase experiment productivity.

- Improved connections between the SMA sample wire and the steel leader wire would allow application of increased forces on the sample.
- Addition of an ice bath in the water inlet hose would increase cooling rates when below sample temperatures of 50°C.
- Insulation of exposed top and bottom plate surfaces and threaded connection rods would minimize heat loss and energy consumption during experiments.
- Developing a cooling method for the top plate would ensure that both the top and bottom plates undergo cooling at similar rates, thus improving the controllability of the wire sample's environment.

Further research is needed to extend the capabilities and accuracy of the experimental apparatus and methods used in its employment.

Appendix A

MANUFACTURER DATA

Manufacturer Data for Equipment

Model 561 Electro-Optical Biaxial Tracking System (Optron™)

Model 561 Control Unit:

Model 806 Tracking Head:

Model 560 Target Illuminator:

Standard Lens Set:

Manufactured by: Optometrix, 30 Hazel Terrace, Westhaven, CT 06525

Oscilloscope: Hewlett Packard Model 54600A

Bandwidth: 10MHz

Dual Channel

120V- 240V

27ns Sampling for Repetitive Waveforms

2mV – 5mV Input Sensitivity

Internally and Externally Triggerable

1.0% Accuracy

DC Power Supply: Harrison Laboratories Model 6200A Power Supply

120VAC / 60Hz

Settings: Off; 1.5A 0-20V; and 750mA 0-40V

Voltage Display: 0-40V Scale

Amperage Display: 0-1.8A Scale

Displacement Transducer: Hewlett-Packard Model 7DCDT-1000 (FU)

DC Input – DC Output

Linearity Error Less Than 0.5%

Stroke: $\pm 76.2\text{mm}$

Temperature Limits: $< 140^{\circ}\text{F}$

Core Diameter: 3.05mm

Manufactured by: Hewlett-Packard Andover Division

1776 Minuteman Road, Andover, MA 01810

Hot Plate: Corning Model PC-420 Laboratory Stirrer / Hot Plate

120VAC 60 Hz 698 Watts

Temperature Stability: $\pm 1.0^{\circ}\text{C}$

Stir Rate: 50 – 150 rpm

With Remote Temperature Sensor and

254mm Stainless Steel Immersion Probe

Heat Gun: Steinel Model HL1502S Hot Air Gun

120 VAC With: 2 Hot Air Stages (1050°F and 800°F)

2 Air Flow Speeds (8.8cfm and 17.6cfm)

1 Cold Air Stage (11.3cfm)

Thermometer: 305mm General Purpose Single Temperature Range

Total Immersion Thermometer

Mercury Filled with Yellow Back

Temperature Range: -20°C to 110°C in 1°C Increments

Accuracy: $\pm 1.0^{\circ}\text{C}$

Manufactured by: HB, USA. Stock No. 6106-026

Micrometer: Mitutoyo Shock Proof Micrometer, Part #505-645-50

Stainless Hardened 12" Caliper Range in 0.001" Increments

Manufactured by: Mitutoyo Corporation

31-19 Shiba 5-Chame, Minato-Ku-Tokyo 108, Japan

Manufacturer Data for SMA Wire, Fittings and Miscellaneous Items

SMA Wire: Flexinol #3-136 Muscle Wires Super Sample Kit

Sizes Provided: 20cm each of 037 μm , 050 μm , 100 μm , 150 μ and 250 μm

Wires in two temperatures: LT (70°C) and HT (90°C) plus crimps

Manufactured by: Mondo-Tronics, Inc., 4285 Redwood Highway #226

San Rafael, CA 94960

Connector Sleeves: Size 3 Berkley™ Wire Leader Connector Sleeves

25 – 50 Pound Test Rating

Stock # 028632018415

Manufactured by: Berkley Outdoor Technologies Group

1900 18th Street, Sprit Lake, IA 51360-1099

Steel Leader Wire: 18" Long Steel Fishing Leader #WL18 –

Leader and Steel Hooks

Stock # 016201

Made in China

Zinc Bar: Square Rod Stock, ½" x 3' Plain Part # 20140

Manufactured by: Crown Bolt, Inc.

Plastic Cylinder: Cast Acrylic. Part #8486K233 (1997 McMaster Catalog)

Length: 300mm

Inside Diameter: 203mm

Wall Thickness: 14.0mm

Screws: 8 x 32 x ½" Machine Screws Part #33461

and 6 x 32 x ½" Machine Screws Part #33371

Flat Head, Slotted, Stainless Steel

Manufactured by: Crown Bolt, Inc. Cerritos, CA 90703

Heat Pipe: 1-1/4" x 6" Galvanized Steel Pipe Nipple. Part #10750

Quantity: 1 each

With: 1-1/4" x 90° Elbows Part # 60006 Quantity: 2 each

Manufactured by: Southland Pipe Nipples, Inc.

Heat Pipe Insulation: Aluminized Ceramic Insulation Strip

Construction: White Aluminum Oxide Based Ceramic Fibers Bonded to a
2mil Strip of Aluminum Foil

Performance: Working Temperature: 2300°F

Melting Point: 3200°F

Order in: 1" Wide x 1" Thick x 12' Roll Part #: 9379K91 (McMaster)

Copper Coil: General Purpose Copper Coil. Part #2004864302080

Dimensions: 1/4" O.D., 20 Feet Long

Manufactured by: Anderson-Barrows Metals Corporation
Palmdale, CA 93550

Compression Adapter: Part #BP62-FM W94 Quantity: 2 each

1/4" x 3/8" Female Compression to Male Compression Adaptor

Manufactured by: Anderson-Barrows Metals Corporation
Palmdale, CA 93550

Hose Barb: 3/8" I.D. Hose x 3/8" Male Pipe Thread Quantity: 2 each

Part # P298

Manufactured by: PlumbShop, Novi, MI 48375-5331

Heater Hose: Gates Safety Stripe Heater Hose, 3/8" (9.5mm) I.D.

Part # M03248 B100

Characteristics: Fiber Reinforced, 0.15" Thick Walls

Made in U.S.A.

Quantity: 8.0 Feet (2.44m)

Thermal Grease: Dow Corning 340 Silicone Heat Sink Compound

Net Wt. 5.0 oz. / 142g

Manufactured by: Dow Corning Corporation, Midland, MI 48640

Two-Part Epoxy: JB Weld™ 1.0 oz. Tube Set

50% - 50% mix of Epoxy Steel Resin and Epoxy Steel Hardener

Manufactured by: JB Weld Corporation, P.O. Box 483,

Sulphur Springs, TX 75843

Appendix B

CALIBRATION OF INSTRUMENTS :

Optron™ Electro-Optical Biaxial Tracking System Calibration

Descriptions of calibration methods in this section are adapted and condensed from the Optron Operations Manual (Reference (23)), which provided guidance for calculations pertaining to Optron setup.

Calculations for which focal length to use for the Optron Optical Scanner were performed as described in pages 3-2 through 3-6 of Reference (23). The size of tube selected for experiments in this report was 136mm focal length, which required the lens and lens extender assembly to have a length of 100mm. The length of the lens assembly was not changed during the course of experiments. The working distance from the lens to the black and white optical target on the lever was 455mm, and this distance was verified during setup of each experiment to ensure that the target was sharply focused in the optical scanner's viewfinder. The vertical distance of the scanner above the floor was adjusted through use of a supporting tripod so that the scanner's lens was level with the black and white Optron target on the lever.

To perform output calibration of the Optron Optical Tracking System, the Optron System was first set up as shown in Figure 9 in Chapter 2. The Optron Controller was set up per manufacturer recommendations for tracking a target with vertical movement. The environmental chamber was set up in position on

the hot plate with the weight application lever on the fulcrum. The black and white optical target shown in Figure 7 was attached to the end of the lever with adhesive tape. The target's black side was on the bottom and the white side was on top. The lever was not connected to the SMA wire at this point; the lever was supported by a block ('blocked') above the upper surface of the top plate so that it remained immobile.

The size of the optical target and distance from the Optron optical viewer was such that the black and white target completely filled the Optron's viewing screen. The dividing line between black and white on the target was aligned with the horizontal centerline in the Optron viewer by moving the optron optical scanner up and down vertically on the tripod to establish a zero point, at which time the scanner was locked in place with the tripod's securing levers. The distance from the upper surface of the top plate to the horizontal division between black and white on the target was measured with a micrometer, and the voltage output of the oscilloscope was read.

To establish an upper bound, the lever was pivoted vertically up until the target's black and white dividing line corresponded with the upper horizontal line in the Optron's viewing field and blocked in place. The oscilloscope's output voltage was recorded, along with the vertical distance of the target's horizontal line above the upper surface of the top plate. Similarly, to establish a lower bound, the target's black/white boundary was rotated downward until it reached the lower horizontal line in the Optron's viewing field, where the lever was

blocked in place, and measurements of oscilloscope voltage and target black/white boundary distance above the top plate were recorded.

Target Black/White Interface Location	Target Black/White Interface Distance Above Top Plate	Optron Voltage Output
At Upper Bound in Optron Viewing Screen	3.907 inches	+ 5.26 volts
At Lower Bound in Optron viewing Screen	2.959 inches	- 5.00 volts

Table B.1: Optron Calibration Table.

To obtain a conversion factor from Optron output voltage to lever displacement:

$$\begin{aligned} &(\text{Change in Displacement}) / (\text{Change in Voltage}) = \\ &(3.907\text{in} - 2.959\text{in}) / (+5.26\text{V} - (-5.00\text{V})) = 0.0924 \text{ inches / Volt} \end{aligned}$$

Which converted to a metric conversion factor of 0.0023464 mm/mV that was applied to output voltage readings from the oscilloscope to change from Optron voltage output to vertical lever displacement.

Optron Voltage Drift Experiment

At the conclusion of Experiment #2, while performing other calculations after running the experiment, the Optron was left running with the lever blocked in place, and therefore, without changes to displacement input. Over a period of 30 minutes, a slight change in output voltage was noticed, so a separate experiment was conducted to quantify the change in the Optron's output voltage

as a function of time. A few days after Experiment #2 was conducted, a test was run to determine Optron output voltage change assuming a constant target input position, and the results of that experiment are shown in the figure below.

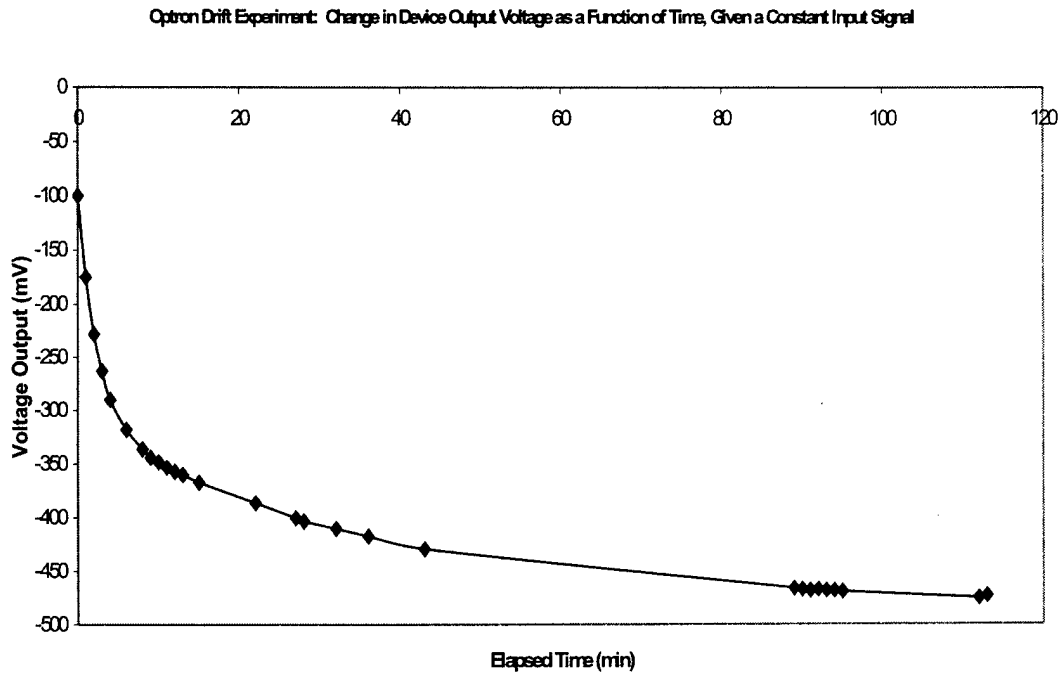


Figure B.1: Optron output voltage drift as a function of time.

Over the first 20 minutes, the Optron reached 80% of its quasi-steady state value, and reached 95% of its stabilized value after 70 minutes. The cause of this voltage drift was unknown, so separate experiments on SMA wire samples were run using a displacement transducer to measure SMA wire displacement and verify findings obtained from the Optron.

Displacement Transducer Calibration

To calibrate the displacement transducer, the environmental chamber and surrounding accessories were set up as shown in Figure 10. The displacement

transducer was fastened to a metal stand separate from the environmental chamber and aligned so that the displacement transducer's probe contacted the top surface of the weight application lever. The lever was blocked in place and the distance of the lever arm above the top plate was measured and recorded along with the displacement transducer's output voltage. The lever arm was displaced a small amount, with measurements of height above the top plate and output voltage measured iteratively until a sufficient range was obtained above and below a level 'zero point.' The results of that calibration are shown in Figure B.2.

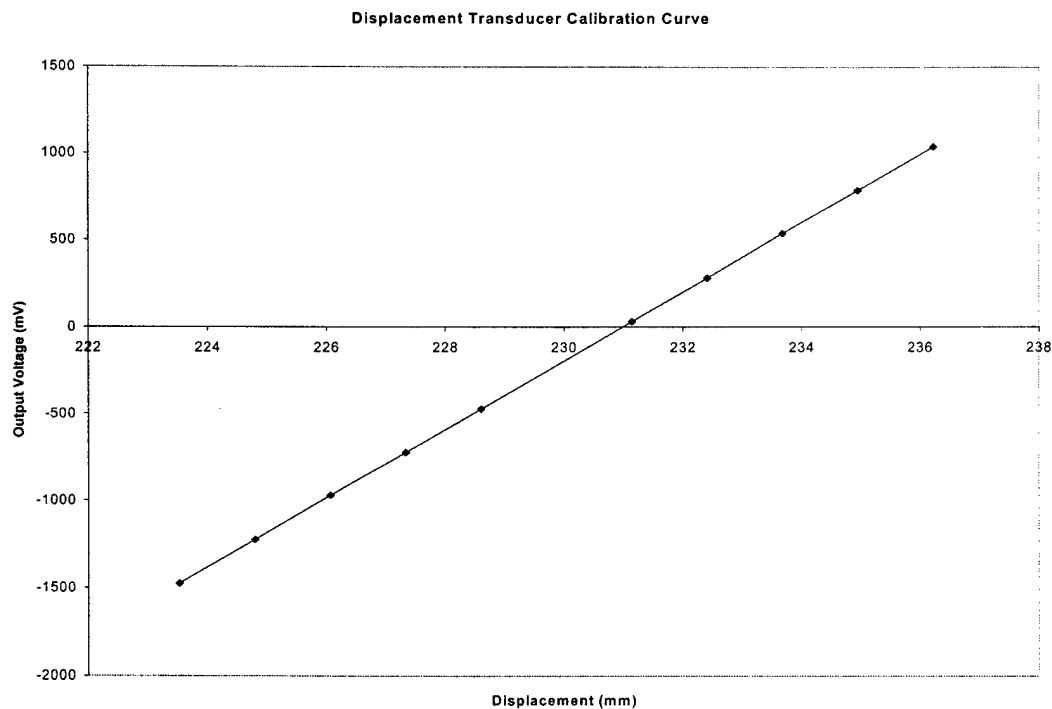


Figure B.2: Displacement transducer calibration curve.

Output voltage was scaled to vertical displacement by using a method similar to that used for the Optron, using change in displacement divided by change in voltage. From spreadsheet calculations, the average value of the slope

of the calibration curve in Figure B.2 was 197.9 mV/mm or 0.00505 mm/mV that was applied to output voltage readings from the oscilloscope to change from voltage output to vertical lever displacement.

When using the displacement transducer, a second calibration must be made to obtain a conversion factor that relates displacement transducer vertical motion to SMA wire assembly vertical motion. Figure B.3 provides a graphic view of the conversion calculation that was required. The distance from the displacement transducer probe to the lever's fulcrum (Distance F-T) was not always identical to the distance from the SMA wire to the fulcrum (Distance F-W), and the conversion factor that is calculated below was applied to voltage output readings from the displacement transducer for all runs in Experiment #3.

$$\text{Distance F-T} = 4.796\text{in} = 121.8184\text{mm}$$

$$\text{Distance F-W} = 4.021\text{in} = 102.1334\text{mm}$$

Assuming a 1.0in vertical downward displacement on the transducer end of the lever,

$$\tan(\theta) = (\text{opposite}) / (\text{adjacent}) = 1.0 / 4.796 \quad \text{or} \quad \theta = 11.7778^\circ$$

Applying simple geometry with an angle of $\theta = 11.7778^\circ$ and an F-W distance of 4.021in,

$$\begin{aligned}\tan(11.7778^\circ) &= (\text{Wire End Vertical Displacement}) / (\text{F-W Distance}) \\ &= (\text{Wire End Vertical Displacement}) / (4.021\text{in})\end{aligned}$$

or $\text{Wire End Vertical Displacement} = (0.8384\text{inches} / 1.0 \text{ inch})$
that yields a unitless conversion factor of 0.8384 to convert from transducer vertical displacement to SMA wire vertical displacement.

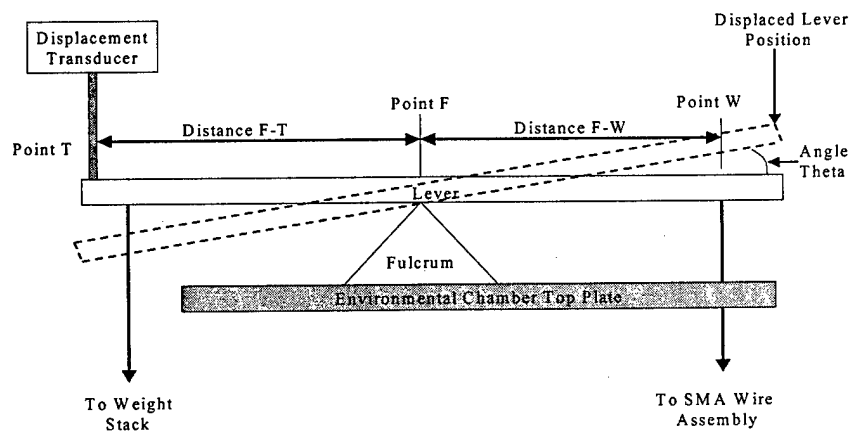
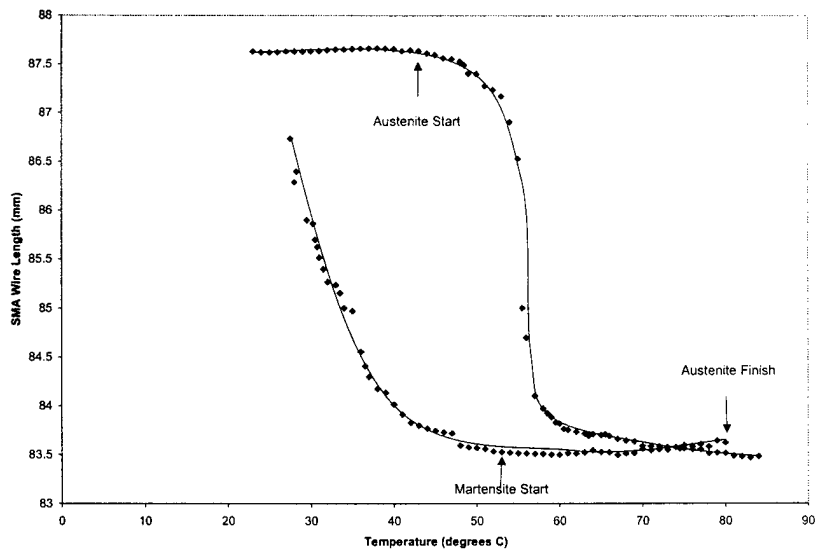


Figure B.3: Calibration of displacement transducer with SMA wire motion.

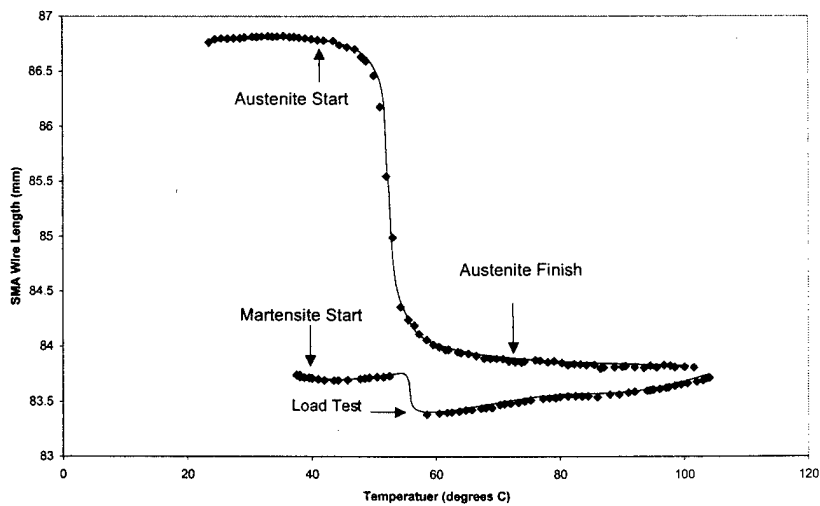
Appendix C

EXPERIMENTAL RESULTS – Hysteresis Curves From Heat Cycling Runs

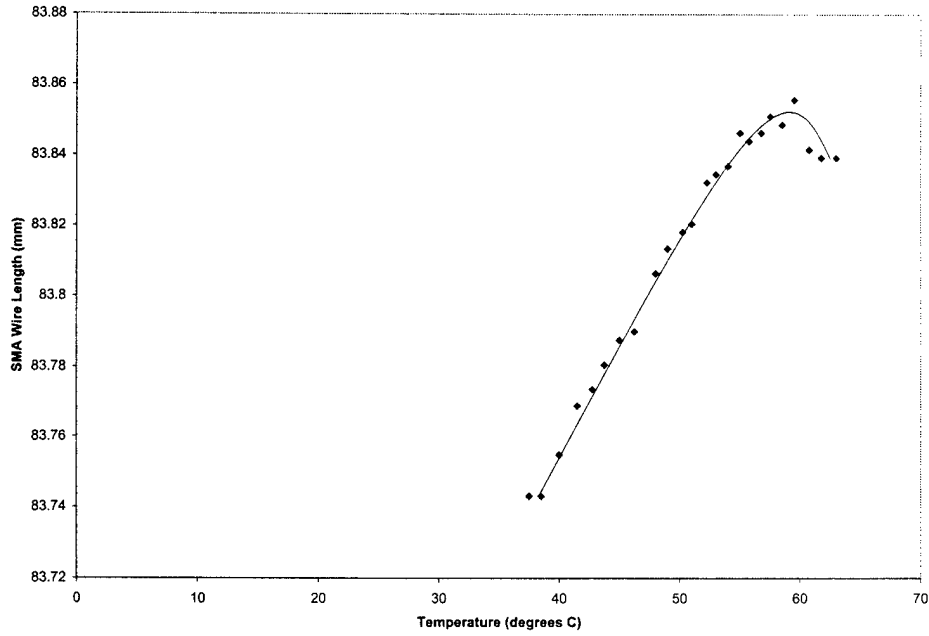
Experiment #1 Run #2: 150 LT Muscle Wire, 87.63mm Effective Length (at Start), 49.7 grams Tare Mass, Length Change in Response to Temperature



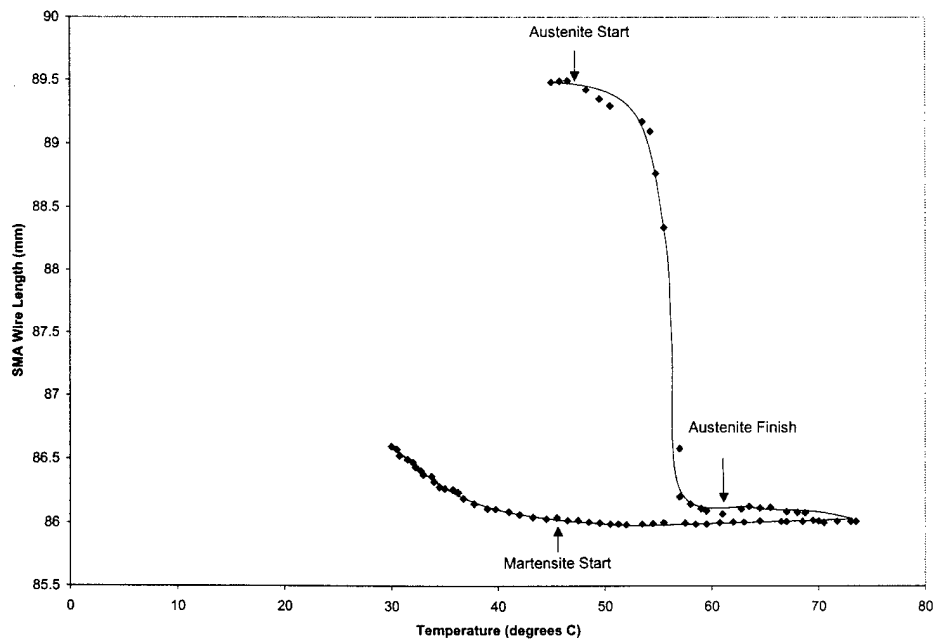
Experiment #2 Run #2: 150 HT Muscle Wire, 86.79mm Effective Length (at Start), 49.7 grams Tare Mass, Length Change in Response to Temperature



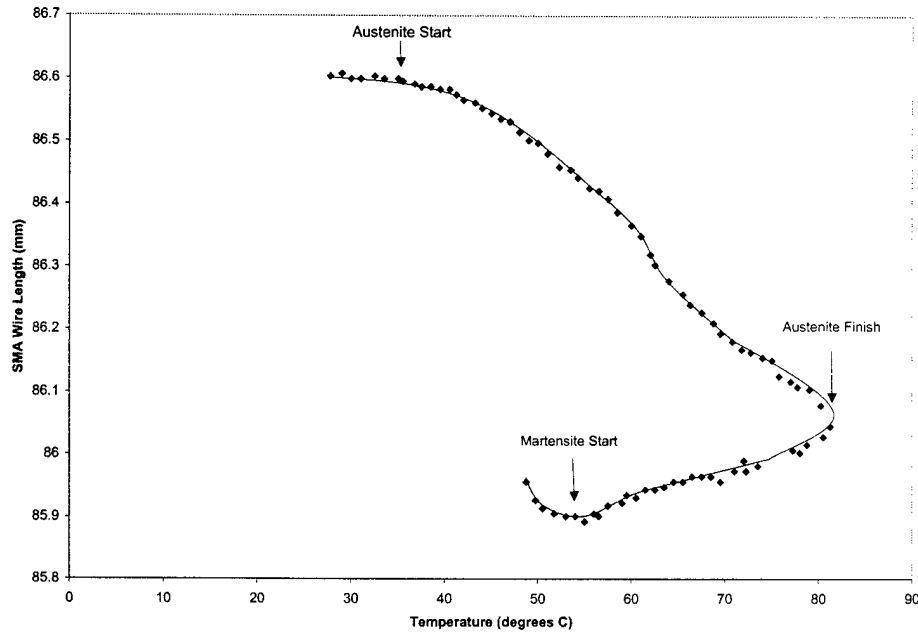
Experiment #2 Run #4: 150 HT Muscle Wire, 86.79mm Effective Length (at Start), 49.7 grams Tare Mass, Length Change in Response to Temperature



Experiment #3 Run #1: 250 LT Muscle Wire, 89.48mm Effective Length, 28.3 grams Tare Mass, Length Change in Response to Temperature

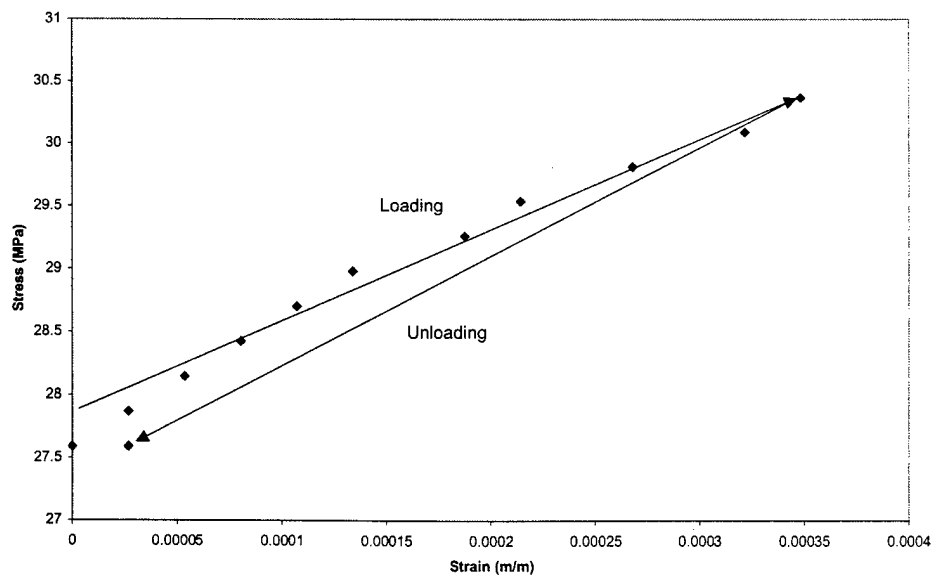


Experiment #3 Run #4: 250 LT Muscle Wire, 89.48mm Effective Length (at Start), 28.3 grams Tare Mass,
Length Change in Response to Temperature

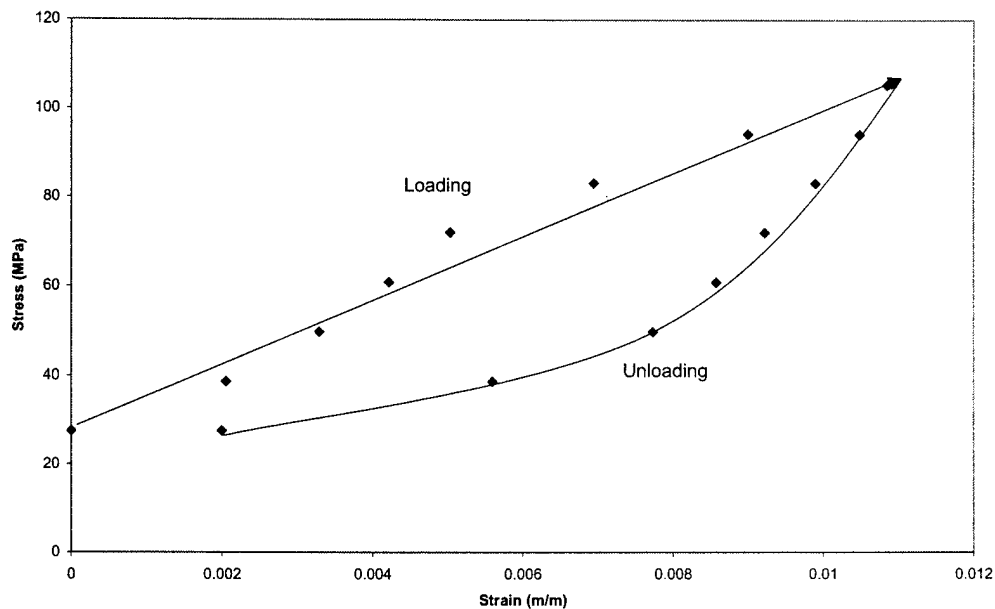


Stress-Strain Curves From Load Cycling Runs

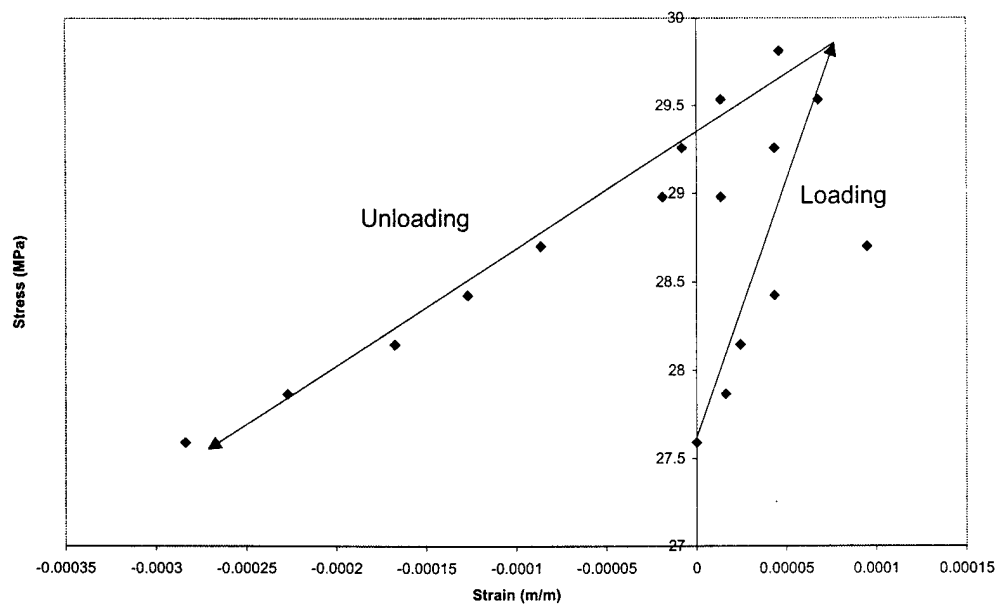
Experiment #1 Run #1: 150 LT Muscle Wire, 87.63mm Effective Length (at Start), 49.7 grams
Tare Mass, Stress - Strain Diagram with Loads Applied at 23 Degrees Celsius



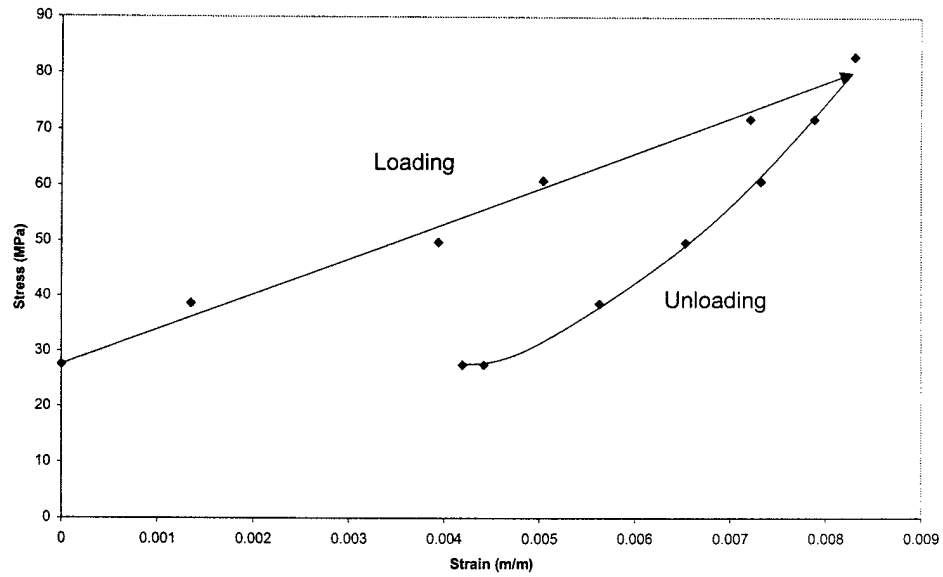
Experiment #1 Run #3: 150 LT Muscle Wire, 87.63mm Effective Length (at Start), 49.7 grams
Tare Mass, Stress - Strain Diagram with Loads Applied at 83 Degrees Celsius



Experiment #2 Run #1: 150 HT Muscle Wire, 86.79mm Effective Length (at Start), 49.7 grams
Tare Mass, Stress - Strain Diagram with Loads Applied at 23 Degrees Celsius



Experiment #2 Run #3: 150 HT Muscle Wire, 86.79mm Effective Length (at Start), 49.7 grams Tare Mass, Stress - Strain Diagram with Loads Applied at 55 Degrees Celsius



Experiment #3 Run #2: 250 LT Muscle Wire, 89.48mm Effective Length (at Start), 28.3 grams Tare Mass, Stress - Strain Diagram with Loads Applied at 23 Degrees Celsius

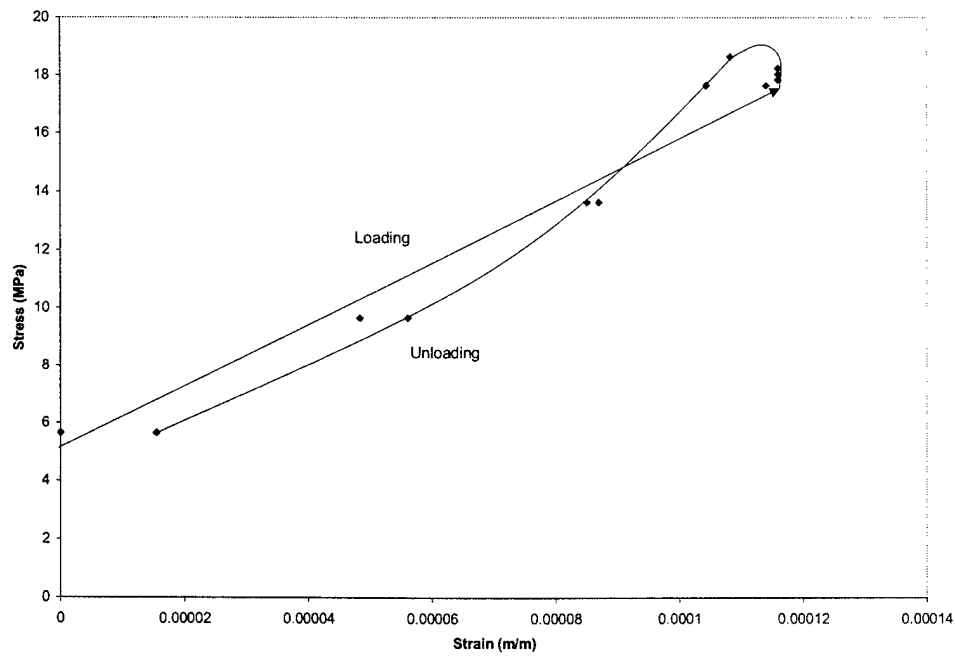


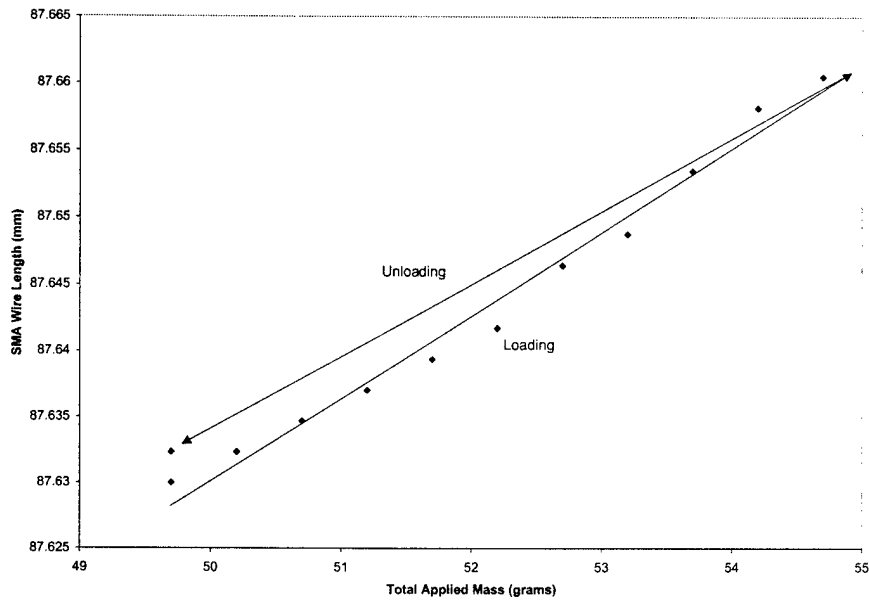
Figure 1 is a stress-strain plot showing the loading and unloading behavior of a material. The y-axis represents Stress (MPa) from 0 to 25, and the x-axis represents Strain (m/m) from 0 to 0.00016. The loading curve is a straight line starting at (0, 5) and ending at (0.00014, 22). The unloading curve is a straight line starting at (0.00014, 22) and ending at (0.00006, 5). The plot shows a hysteresis loop, indicating that the material's behavior is not perfectly elastic.

Strain (m/m)	Stress (MPa)	Curve Type
0.00000	5.0	Loading
0.00001	5.5	Loading
0.00002	6.0	Loading
0.00003	6.5	Loading
0.00004	7.0	Loading
0.00005	7.5	Loading
0.00006	8.0	Loading
0.00007	8.5	Loading
0.00008	9.0	Loading
0.00009	9.5	Loading
0.00010	10.0	Loading
0.00011	10.5	Loading
0.00012	11.0	Loading
0.00013	11.5	Loading
0.00014	12.0	Loading
0.00015	12.5	Loading
0.00016	13.0	Loading
0.00017	13.5	Loading
0.00018	14.0	Loading
0.00019	14.5	Loading
0.00020	15.0	Loading
0.00021	15.5	Loading
0.00022	16.0	Loading
0.00023	16.5	Loading
0.00024	17.0	Loading
0.00025	17.5	Loading
0.00026	18.0	Loading
0.00027	18.5	Loading
0.00028	19.0	Loading
0.00029	19.5	Loading
0.00030	20.0	Loading
0.00031	20.5	Loading
0.00032	21.0	Loading
0.00033	21.5	Loading
0.00034	22.0	Loading
0.00035	22.5	Loading
0.00036	23.0	Loading
0.00037	23.5	Loading
0.00038	24.0	Loading
0.00039	24.5	Loading
0.00040	25.0	Loading
0.00041	25.5	Loading
0.00042	26.0	Loading
0.00043	26.5	Loading
0.00044	27.0	Loading
0.00045	27.5	Loading
0.00046	28.0	Loading
0.00047	28.5	Loading
0.00048	29.0	Loading
0.00049	29.5	Loading
0.00050	30.0	Loading
0.00051	30.5	Loading
0.00052	31.0	Loading
0.00053	31.5	Loading
0.00054	32.0	Loading
0.00055	32.5	Loading
0.00056	33.0	Loading
0.00057	33.5	Loading
0.00058	34.0	Loading
0.00059	34.5	Loading
0.00060	35.0	Loading
0.00061	35.5	Loading
0.00062	36.0	Loading
0.00063	36.5	Loading
0.00064	37.0	Loading
0.00065	37.5	Loading
0.00066	38.0	Loading
0.00067	38.5	Loading
0.00068	39.0	Loading
0.00069	39.5	Loading
0.00070	40.0	Loading
0.00071	40.5	Loading
0.00072	41.0	Loading
0.00073	41.5	Loading
0.00074	42.0	Loading
0.00075	42.5	Loading
0.00076	43.0	Loading
0.00077	43.5	Loading
0.00078	44.0	Loading
0.00079	44.5	Loading
0.00080	45.0	Loading
0.00081	45.5	Loading
0.00082	46.0	Loading
0.00083	46.5	Loading
0.00084	47.0	Loading
0.00085	47.5	Loading
0.00086	48.0	Loading
0.00087	48.5	Loading
0.00088	49.0	Loading
0.00089	49.5	Loading
0.00090	50.0	Loading
0.00091	50.5	Loading
0.00092	51.0	Loading
0.00093	51.5	Loading
0.00094	52.0	Loading
0.00095	52.5	Loading
0.00096	53.0	Loading
0.00097	53.5	Loading
0.00098	54.0	Loading
0.00099	54.5	Loading
0.00100	55.0	Loading
0.00101	55.5	Loading
0.00102	56.0	Loading
0.00103	56.5	Loading
0.00104	57.0	

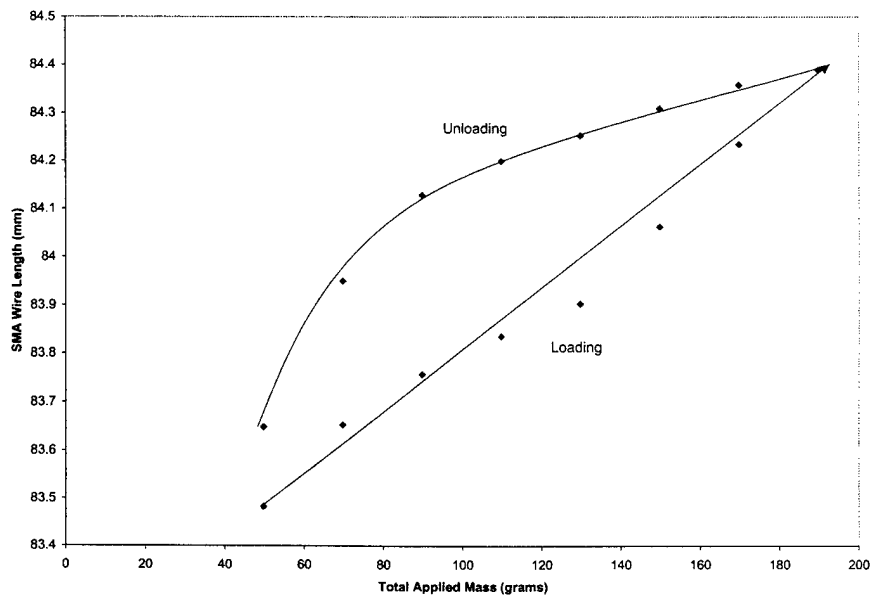
Figure 10 is a stress-strain graph showing the behavior of a connector under cyclic loading. The y-axis represents Stress (MPa) from 0 to 140, and the x-axis represents Strain (m/m) from 0 to 0.003. The graph shows a loading curve (solid line with dots) and an unloading curve (dashed line with dots). The loading curve starts at (0,0) and rises to a peak stress of approximately 115 MPa at a strain of 0.0026 m/m, labeled "Connector Failure". The unloading curve starts at the peak and returns to the origin. The area between the loading and unloading curves is labeled "Loading Second Time" and "Unloading First Time".

Load – Displacement Curves from Load Cycling Runs

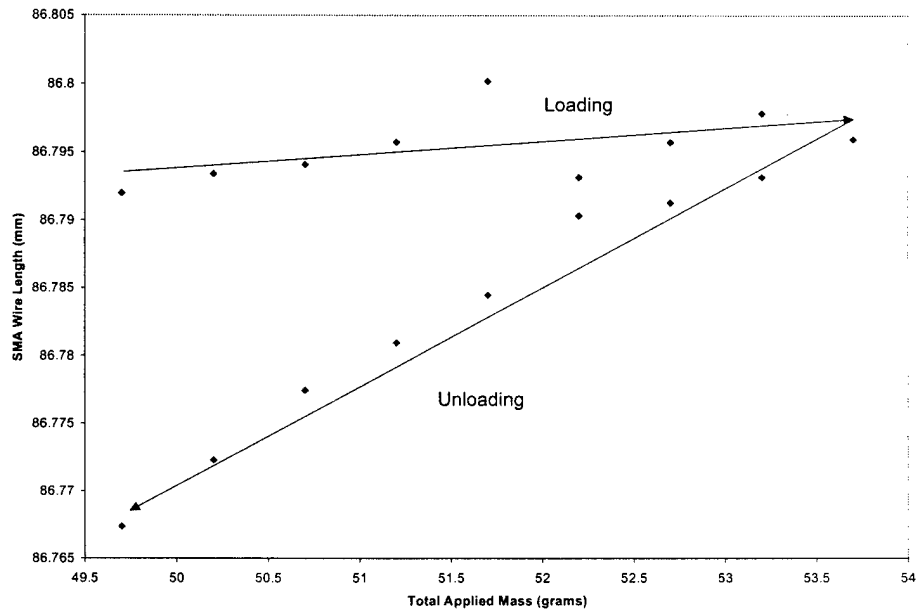
Experiment #1 Run #1: 150 LT Muscle Wire, 87.63mm Effective Length (at Start), 49.7 grams Tare Mass,
Length Change with Applied Mass at 23 Degrees Celsius



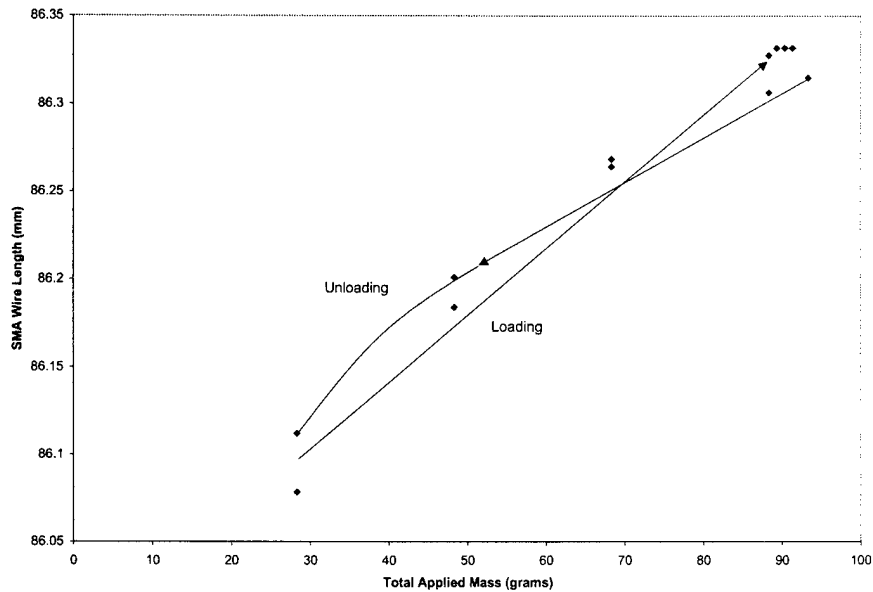
Experiment #1 Run #3: 150 LT Muscle Wire, 87.63mm Effective Length (at Start), 49.7 grams Tare Mass,
Length Change with Applied Mass at 83 Degrees Celsius



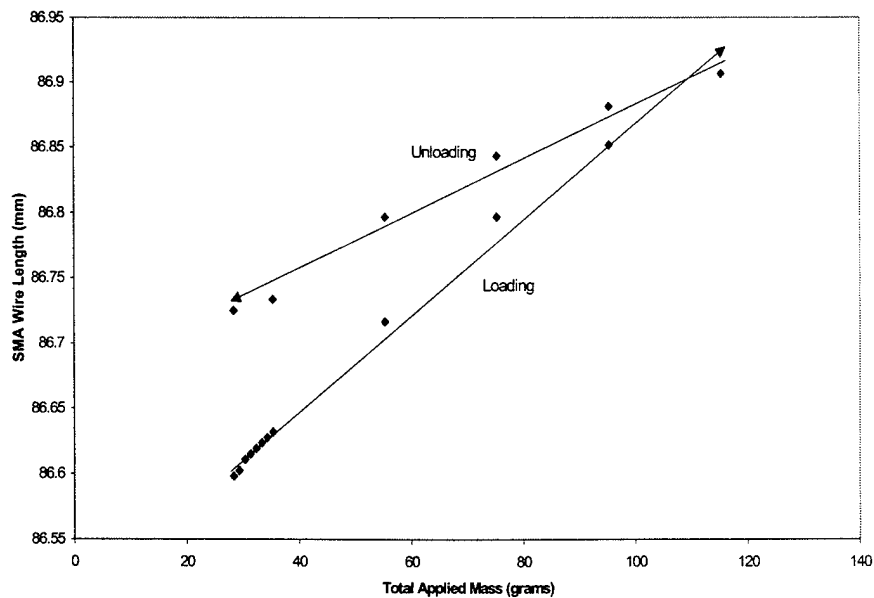
Experiment #2 Run #1: 150 HT Muscle Wire, 86.79mm Effective Length (at Start), 49.7 grams Tare Mass,
Length Change with Applied Mass at 23 Degrees Celsius



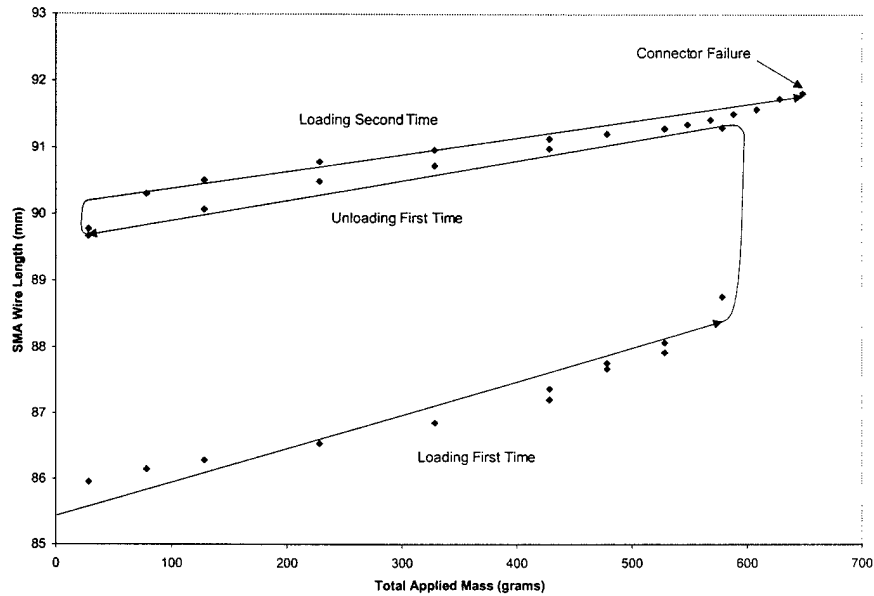
Experiment #3 Run #2: 250 LT Muscle Wire, 89.48mm Effective Length (at Start), 28.3 grams Tare Mass,
Length Change with Applied Mass at 74 Degrees Celsius



Experiment #3 Run #3: 250 LT Muscle Wire, 89.48mm Effective Length (at Start), 28.3 grams
Tare Mass, Length Change with Applied Mass at 30 Degrees Celsius

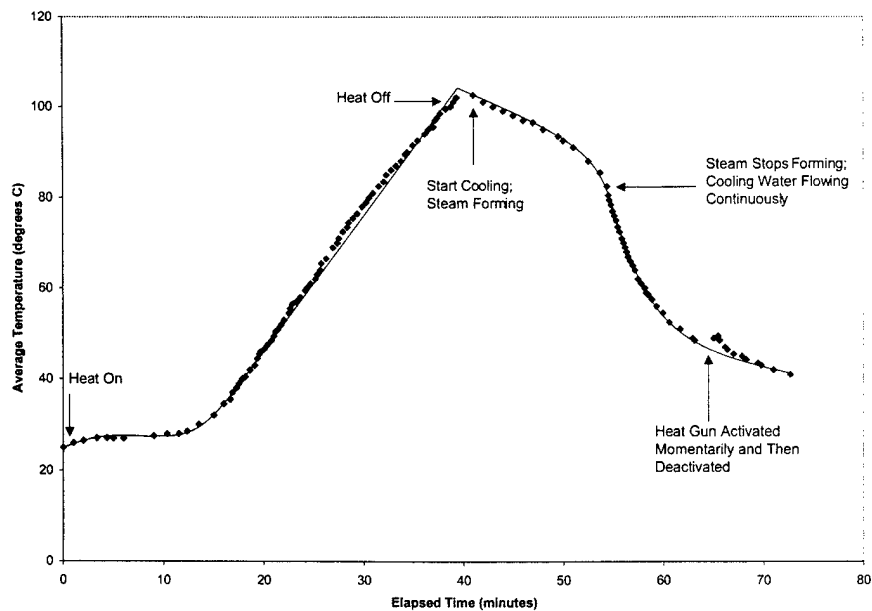


Experiment #3 Run #5: 250 LT Muscle Wire, 89.48mm Effective Length (at Start), 28.3 grams Tare Mass, Length Change with Applied Mass at 47 Degrees Celsius

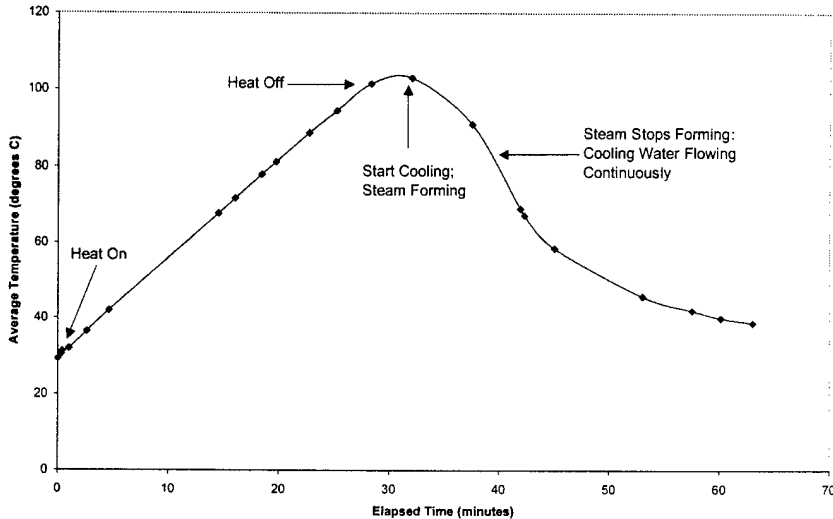


Temperature Curves

Functional Test: Environmental Chamber Temperature as a Function of Time



Experiment #2 Run #2: Environmental Chamber Temperature as a Function of Time



EXPERIMENTAL RESULTS TABLE								
Transition Temperatures								
Low Temperature Wire	Manufacturer's Data	Experiment #1 Run #2	Experiment #3 Run #1	Experiment #3 Run #4	Lengths at Each State	Experiment #1 Run #2	Experiment #3 Run #1	Experiment #3 Run #4
SMA Sample Size / Type	150 LT / 250 LT	150 LT	250 LT	250 LT				
Austenite Start (deg C)	68	43	47	35	Exp start Length (mm)	87.6	89.5	86.61
Austenite Finish (deg C)	78	80	61	83	Af Length (mm)	83.5	86.15	86.08
Martensite Start (deg C)	52	54	45	53	Ms Length (mm)	83.5	86	85.89
Martensite Finish (deg C)	42	n/a	n/a	n/a	Final Length (mm)	86.7	86.6	85.95
					Maximum Change (mm)	4.1	3.5	0.72
					Max Change (%)	0.046803653	0.039106145	0.008313128
Transition Temperatures								
High Temperature Wire	Manufacturer's Data	Experiment #2 Run #2			Lengths at Each State	Experiment #1 Run #2		
SMA Sample Size / Type	150 HT	150 HT						
Austenite Start (deg C)	88	42			Exp start Length (mm)	86.77		
Austenite Finish (deg C)	98	72			Af Length (mm)	83.8		
Martensite Start (deg C)	72	40			Ms Length (mm)	83.7		
Martensite Finish (deg C)	62	n/a			Final Length (mm)	83.7		
					Maximum Change (mm)	3.07		
					Max Change (%)	0.035380892		
Young's Modulus Analysis								
	Manufacturer's Data	Experiment #1 Run #1	Experiment #1 Run #3	Experiment #2 Run #1	Experiment #2 Run #3	Experiment #3 Run #2	Experiment #3 Run #3	Experiment #3 Run #5
Young's Modulus (Gpa)		(Gpa)						
Austenite	75							
Martensite	28							
During Loading		7.228	7.128	28.636	6.373	10.702	119.587	135.61
During Unloading - Initial		8.673	17.973	6.529	18.194	22.142	204.27	327.03
Unloading, Straight Line			6.739		12.789	13.999		140.17
Average - All Results		7.9505	10.61333333	17.5825	12.452	15.61433333	161.9285	200.9366667
Average - Straight Lines		7.9505	6.9335	17.5825	9.581	12.3505	161.9285	137.89
Load Range (grams)		49.7 - 54.7	49.7 - 189.7	49.7 - 54.7	49.7 - 149.7	28.3 - 92.3	28.3 - 116.3	28.3 - 648.3
Average Temperature (deg C)		23	83	23	55	74	30	47
Wire Type		150 LT	150 LT	150 HT	150 HT	250 LT	250 LT	250 LT
Effective length at Start (mm)		87.63	87.63	86.79	86.79	89.48	89.48	89.48
Length at Start of Exp. Run		87.63	83.48	86.79	83.39	86.08	86.6	85.95
Maximum Length During Run		87.661	84.39	86.8	84.08	86.33	86.91	91.3
Length at End of Exp. Run		87.6325	83.65	86.7675	83.74	86.11	86.73	89.8
Max Stretched Length Change		0.031	0.91	0.01	0.69	0.25	0.31	5.35
Max Strain (m/m)		0.00035376	0.010384571	0.000115221	0.007950225	0.00279392	0.003464461	0.059789897

Bibliography

- (1) Thrasher M A, Shahin A R, Meckl P H, and Jones J D. June 1994. Efficiency Analysis of Shape Memory Alloy Actuators. In *Smart Materials and Structures*, V.3, Nr. 2. IOP Publishing Ltd. 226.
- (2) Wayman C M, and Duerig T W. 1990. An Introduction to Martensite and Shape Memory in Duerig T W, Melton K N, Stockel D, and Wayman C M. 1990. *Engineering Aspects of Shape Memory Alloys*. London: Butterworth-Heinemann Ltd. 4-8.
- (3) Verhoeven, J D. 1975. *Fundamentals of Physical Metallurgy*. John Wiley & Sons, New York. 474.
- (4) Touloukian Y S, Kirby R K, Taylor R E, and Desai P D. 1975. *Thermophysical Properties of Matter – The TPRC Data Series. Vol. 12 – Thermal Expansion – Metallic Elements and Alloys*. Purdue Research Foundation. Plenum Publishing Corporation. New York. 2-1131.
- (5) Otuska K. Introduction to the R-Phase Transition in Duerig T W, Melton K N, Stockel D, and Wayman C M. 1990. *Engineering Aspects of Shape Memory Alloys*. Butterworth-Heinemann Ltd., London. 43.
- (6) Wayman C M, and Duerig T W. 1990. An Introduction to Martensite and Shape Memory in Duerig T W, Melton K N, Stockel D, and Wayman C M. *Engineering Aspects of Shape Memory Alloys*. Butterworth-Heinemann Ltd., London. 11-13.
- (7) Adapted from Wayman C M, and Duerig T W. 1990. An Introduction to Martensite and Shape Memory in Duerig T W, Melton K N, Stockel D, and Wayman C M. *Engineering Aspects of Shape Memory Alloys*. Butterworth-Heinemann Ltd., London. Figure 7, pg. 10, and Duerig T W, and Pelton A R. 1994. Ti-Ni Shape Memory Alloys. In Gergard W, Boyer R, and Collings E W. *Materials Properties Handbook*. ASM International, Materials Park, OH. Figure pg. 1035.
- (8) "Design Aspects of Shape Memory Actuators", Reynaerts D, Van Brussel H. 1998. *Mechatronics* 8: (6) 635-656 September 1998.

- (9) "Memory Alloy Works Best in a Tight Spot." May 1997. Subcon, Miller Freeman PLC, 1997. pg. 28.
- (10) "Silent Cracker that Breaks the Mould." Garner R. November 15, 1990. London Financial Times, Section I, Technology, Pg. 22. The Financial Times Limited, 1990.
- (11) "Explosive Bolt Alternative", Lavitt M O. November 7, 1994. Aviation Week and Space Technology, vol. 141, No. 119, pg. 79. McGraw-Hill, Inc. 1994.
- (12) "Shape Memory Alloys Top List for Newly Reconfigured Darpa", Chase M. April 10, 1997. Business and Industry, pg. 10A. And American Metal Market Aerospace Metals Supplement. Responsive Database Services, Inc. and Cahners Business Information. 1997.
- (13) "Shaping Quieter Rotors With Smart Materials", Flinn E D. July, 1998. Aerospace America, pg. 24. American Institute of Aeronautics and Astronautics, Inc. 1998.
- (14) Hodgson D E. 1990. Using Shape memory for Proportional Control in Duerig T W, Melton K N, Stockel D, and Wayman C M. *Engineering Aspects of Shape Memory Alloys*. Butterworth-Heinemann Ltd. London. 362.
- (15) Duerig T W and Pelton A R. 1994. "Ti-Ni Shape Memory Alloys" in Welsh G, Boyer R, and Collings E W. *1994 Materials Properties Handbook - Titanium Alloys*. ASM International, Materials Park, OH. 1036-1037.
- (16) Funakubo H. *Precision Machinery and Robotics, Volume 1, Shape Memory Alloys*. 1987. OPA (Amsterdam) B. V. Gordon and Breach Science publishers, New York. 185.
- (17) Yaeger J R. 1990. Electrical Actuators Alloy Selection, Processing and Evaluation in Duerig T W, Melton K N, Stockel D, and Wayman C M. 1990. *Engineering Aspects of Shape Memory Alloys*. Butterworth-Heinemann Ltd., London. 233.
- (18) Yaeger J R. 1990. Electrical Actuators Alloy Selection, Processing and Evaluation in Duerig T W, Melton K N, Stockel D, and Wayman C M. 1990. *Engineering Aspects of Shape Memory Alloys*. Butterworth-Heinemann Ltd., London. 219.

- (19) "A Technician at Heart, Eric Weynant's Company Develops Applications for Shape Memory Alloys", Warwick L. February 27, 1995. The Gazette (Montreal) pg. C3. Southam Inc. 1995.
- (20) "Metal Hands With Human-Like Reflexes; Hitachi Uses Memory Alloys", Walton P. December 8, 1993. London Financial Times, Section I, Technology, pg. 8. The Financial Times Limited. 1983.
- (21) "Improvement of the Response of an SMA Actuator Using a Temperature Sensor", Kuribayashi K. 1991. International Journal of Robotics Research. 10: (1) 13-20 Feb 1991.
- (22) "Muscle Wires", Mondo-Tronics, Inc. Manufacturer's Information Sheet for #3-136 Muscle Wires Sample Kit. Mondo-Tronics, San Rafael CA. 1-4.
- (23) "Model 561 Electro-Optical Biaxial Tracking System Operations Manual", Optometrix Corporation. 1982. Optometrix Corporation, Westhaven, CT. pg. 1-1 to 2-4.
- (24) "Equipment Note - 7DCDT and 24DCDT Displacement Transducers", 1990. Hewlett-Packard Andover Division, Andover, MA. Pg. 1-2.
- (25) Askeland, D R. 1984. *The Science and Engineering of Materials*. Wadsworth, Inc., Belmont, CA. 132-133.

Vita

John A. Zulick was born on September 27, 1965 in Bloomsburg Pennsylvania to Anne L. Zielinski and Robert J. Zulick, Sr. After attending Shamokin Area High School, he received an appointment to the United States Naval Academy in Annapolis, Maryland, where he received a Bachelor's Degree in Mechanical Engineering and a commission as an Ensign in the United States Navy in May 1987. After a year of training in San Diego, CA, he reported to the USS Haleakala (AE-25), an ammunition ship homeported in Apra Harbor, Guam.

In October 1991, Lieutenant Commander Zulick transferred to the Navy's Civil Engineer Corps, subsequently serving Naval Facilities Engineering Command's Western Division as Assistant Resident Officer in Charge of Construction at both Mare Island Naval Shipyard, and Travis Air Force Base, CA.

From 1994 to 1996, he was assigned to Naval Mobile Construction Battalion 74 in Gulfport, Mississippi, deploying to Puerto Rico and Okinawa, Japan. He then studied the Spanish Language at the Defense Language Institute in Monterey, California, before serving as the last Public Works Officer at the U.S. Naval Station Panama Canal from 1996 until the base's closure in 1999. He is married to the former Barbara D. Puckett of Norfolk, VA.

Permanent address: 1461 Wabash Street
Ranshaw, PA 17866

This report was typed by the author.